Title

The proprotein convertase BLI-4 promotes collagen secretion prior to assembly of the Caenorhabditis elegans cuticle.

Journal

PLoS Genetics, 19(9)

Authors

Birnbaum, Susanna
Cohen, Jennifer
Belfi, Alexandra
et al.

Publication Date

2023-09-01

DOI

10.1371/journal.pgen.1010944

Peer reviewed

PLOS GENETICS

RESEARCH ARTICLE

The proprotein convertase BLI-4 promotes collagen secretion prior to assembly of the *Caenorhabditis elegans* cuticle

Susanna K. Birnbaum[1], Jennifer D. Cohen[1], Alexandra Belfi[1], John I. Murray[1], Jennifer R. G. Adams[2], Andrew D. Chisholm[2], Meera V. Sundaram[1]*

1 Department of Genetics, University of Pennsylvania Perelman School of Medicine, Philadelphia, Pennsylvania, United States of America, **2** Departments of Neurobiology and Cell and Developmental Biology, School of Biological Sciences, University of California San Diego, San Diego, California, United States of America

* sundaram@pennmedicine.upenn.edu

Citation: Birnbaum SK, Cohen JD, Belfi A, Murray JI, Adams JRG, Chisholm AD, et al. (2023) The proprotein convertase BLI-4 promotes collagen secretion prior to assembly of the *Caenorhabditis elegans* cuticle. PLoS Genet 19(9): e1010944. https://doi.org/10.1371/journal.pgen.1010944

Editor: Cathy Savage-Dunn, Queens College, CUNY, UNITED STATES

Received: May 29, 2023

Accepted: August 30, 2023

Published: September 18, 2023

Data Availability Statement: All relevant data are within the paper and its Supporting Information files. Additional data that support the findings of this study are publicly available from Github: https://github.com/jisaacmurray/bli4_paper.

Funding: This work was supported by National Institutes of Health grants R35GM136315 to MVS, R35GM134970 to ADC, R35GM127093 to JIM, and training award T32 AR007465 to JDC. The funders had no role in study design, data collection

Abstract

Some types of collagens, including transmembrane MACIT collagens and *C. elegans* cuticle collagens, are N-terminally cleaved at a dibasic site that resembles the consensus for furin or other proprotein convertases of the subtilisin/kexin (PCSK) family. Such cleavage may release transmembrane collagens from the plasma membrane and affect extracellular matrix assembly or structure. However, the functional consequences of such cleavage are unclear and evidence for the role of specific PCSKs is lacking. Here, we used endogenous collagen fusions to fluorescent proteins to visualize the secretion and assembly of the first collagen-based cuticle in *C. elegans* and then tested the role of the PCSK BLI-4 in these processes. Unexpectedly, we found that cuticle collagens SQT-3 and DPY-17 are secreted into the extraembryonic space several hours before cuticle matrix assembly. Furthermore, this early secretion depends on BLI-4/PCSK; in *bli-4* and cleavage-site mutants, SQT-3 and DPY-17 are not efficiently secreted and instead form large intracellular puncta. Their later assembly into cuticle matrix is reduced but not entirely blocked. These data reveal a role for collagen N-terminal processing in intracellular trafficking and the control of matrix assembly *in vivo*. Our observations also prompt a revision of the classic model for *C. elegans* cuticle matrix assembly and the pre-cuticle-to-cuticle transition, suggesting that cuticle layer assembly proceeds via a series of regulated steps and not simply by sequential secretion and deposition.

Author summary

Extracellular matrices coat cell surfaces to affect many aspects of animal biology. Collagens are among the most common constituents of such matrices and often form fibrillar- or mesh-like structures. It is important that these structures form only at the right time and place in the extracellular environment, and not prematurely during intracellular trafficking. Type I collagen matrix assembly typically occurs after proteolytic cleavage to

and analysis, decision to publish, or preparation of the manuscript.

Competing interests: The authors have declared that no competing interests exist.

remove both the N- and C-terminal ends of collagen molecules, and defects in this cleavage can cause a variety of human matrix disorders. Nevertheless, many questions remain about how N-terminal cleavage impacts collagen matrix assembly, particularly within other families of collagens that may be regulated differently than Type I collagen. The nematode *Caenorhabditis elegans* has an exoskeleton or cuticle that is composed of many collagens, and sequential secretion and membrane-proximal assembly of different collagens has been supposed to explain the eventual layered structure of the cuticle. Here we visualized tagged collagens during cuticle assembly and investigated the roles of N-terminal cleavage by characterizing mutants in the predicted collagen protease BLI-4 (a member of the furin/PCSK family) and also mutants in the predicted N-terminal cleavage sites within the tagged cuticle collagens. We observed that collagen secretion normally precedes cuticle matrix assembly by several hours, requiring a new way of thinking about cuticle layer formation. Furthermore, in both *bli-4* mutants and N-terminal cleavage site mutants, collagens were not secreted efficiently and instead formed intracellular puncta. These data reveal an unexpected role for N-terminal cleavage in cuticle collagen secretion, which could be relevant to the cell biology of human matrix disorders.

Introduction

Proteolytic cleavage is a common regulatory step in the assembly of extracellular matrices: Components initially enter the secretory pathway as soluble proproteins and then are cleaved in later secretory compartments or extracellularly to allow their assembly into higher order structures [1–3]. For example, mammalian fibrillar collagens undergo both N-terminal and C-terminal proteolysis in order to convert procollagen to the mature collagen that is found in extracellular fibrils [4–7]. For Type I procollagen, these cleavages depend (at least in part) on members of the ADAMTS and BMP-1/astacin proteinase families, respectively [5,8–10], and failure to appropriately cleave procollagen leads to human connective tissue disorders such as Ehlers-Danlos syndrome Type VII (ED-VII) and Osteogenesis imperfecta [4,9–12]. Some other types of collagens, including transmembrane MACIT collagens (membrane associated collagens with interrupted triple helixes) and *C. elegans* cuticle collagens, are instead N-terminally cleaved at a dibasic site that resembles the consensus for furin or other proprotein convertases of the subtilisin/kexin (PCSK) family [13–17]. However, evidence for the importance of specific PCSKs in collagen cleavage is lacking and the functional consequences of such cleavage are not well defined.

Appropriate cleavage of procollagens may facilitate formation of fibrils or other higher order matrix structures at the right place and time, in the presence of appropriate partners. In the case of transmembrane collagens, N-terminal cleavage also would release the ectodomain from the plasma membrane. Unfortunately, potential redundancy and uncertainty about the specific proteinases involved, combined with difficulties in visualizing collagen matrix *in vivo*, have made it challenging to dissect these regulatory mechanisms in most biological systems. For example, while C-terminal cleavage strongly promotes Type I collagen fibril assembly *in vitro* [5,18], there is still uncertainty about the specific role N-terminal cleavage plays in matrix assembly [3,6,7,19]. Unprocessed Type I Pro(N)-collagen can be found extracellularly in cell culture [4,20] and in morphologically abnormal fibrils in ED-VII patients [21,22], leading to the widespread view that N-terminal processing is not essential for collagen secretion or incorporation into fibrils, but rather affects specific aspects of fibril structure. It remains unclear if this is generally true for other types of collagens, including those cleaved by PCSKs. Finally,

some invertebrate fibrillar collagens and many non-fibrillar collagens do not undergo N- or C-terminal cleavage and must rely on other mechanisms to control the time and place of collagen matrix assembly [23,24].

The nematode *Caenorhabditis elegans* has an external body cuticle that consists primarily of collagens, many of which have a predicted transmembrane domain and/or an N-terminal consensus furin cleavage site (CFCS) that could be cleaved by a PCSK [13,25–27]. A new collagenous cuticle matrix is synthesized in the embryo and during each molt between larval stages, and it is always preceded by a transient "pre-cuticle" matrix that contains zona pellucida (ZP) domain proteins and other non-collagen components [28–34]. Therefore, these two matrix types must be assembled and then disassembled in the proper sequence during the molt cycle. These dynamic matrix changes are controlled in part by oscillatory gene expression programs, with pre-cuticle genes peaking relatively early in each molt cycle and different cuticle collagen genes peaking at early, intermediate, or late timepoints, consistent with an extended period of cuticle synthesis and assembly [35–37]. The molt cycle also is controlled by various post-transcriptional mechanisms such as regulated trafficking and proteolysis [38–43]. A BMP1-related astacin proteinase, DPY-31, has been implicated in C-terminal processing of SQT-3 cuticle collagen [44–46], while one or more furin/PCSKs are thought to be responsible for N-terminal processing of many cuticle collagens at the CFCS. The functional importance of N-terminal cleavage is supported by the fact that CFCS mutations in several collagens cause disruptions to cuticle structure [13,14,25].

Here we investigate the roles of *C. elegans* BLI-4, a member of the furin/PCSK family [47], in cuticle assembly. PCSK proteinases cleave secreted or transmembrane substrates immediately following dibasic sites of consensus sequence (R/K) Xn (R/K), where Xn can be 0, 2, 4, or 6 amino acids [48]. Mammals have 9 PCSK family members that differ primarily in their C-terminal domains, which are thought to confer different subcellular localization patterns and/or substrate preferences [48–50]. *C. elegans* has 4 PCSK family members, among which BLI-4 and KPC-1 appear to be the major ones expressed in external epithelial cells, while EGL-3 and AEX-5 are expressed primarily in neurons, muscle, or internal epithelia [51–53]. *kpc-1*, *egl-3*, and *aex-5* mutants are viable and do not have any reported defects in the molt cycle or cuticle [54–56]. In contrast, *bli-4* is an essential gene, and isoform-specific *bli-4(e937)* mutants have blistered adult cuticles, making BLI-4 an excellent candidate for cleaving cuticle collagens [47]. By imaging formation of the first (L1) cuticle in developing wild-type embryos and *bli-4* or cleavage site mutants, we provide evidence that BLI-4-dependent N-terminal processing of specific cuticle collagens promotes their efficient secretion several hours prior to matrix assembly.

Results

Collagen secretion begins several hours before the pre-cuticle to cuticle transition

The collagenous cuticle matrix of *C. elegans* is preceded by a molecularly distinct pre-cuticle apical extracellular matrix (aECM) that it eventually replaces during each molt cycle [57]. To determine the precise timing and sequence of these events for the first pre-cuticle and cuticle, we imaged staged live embryos expressing fluorescently-tagged matrix factors (Fig 1). Tags were located either internally (int), at the N-terminus immediately following the signal sequence (ss), or at the extreme C-terminus, as described in S1 and S2 Table and schematized in the figures below. All of these matrix fusions were generated by CRISPR/Cas9-dependent tagging of the endogenous loci and were functional based on phenotypic assays (Methods).

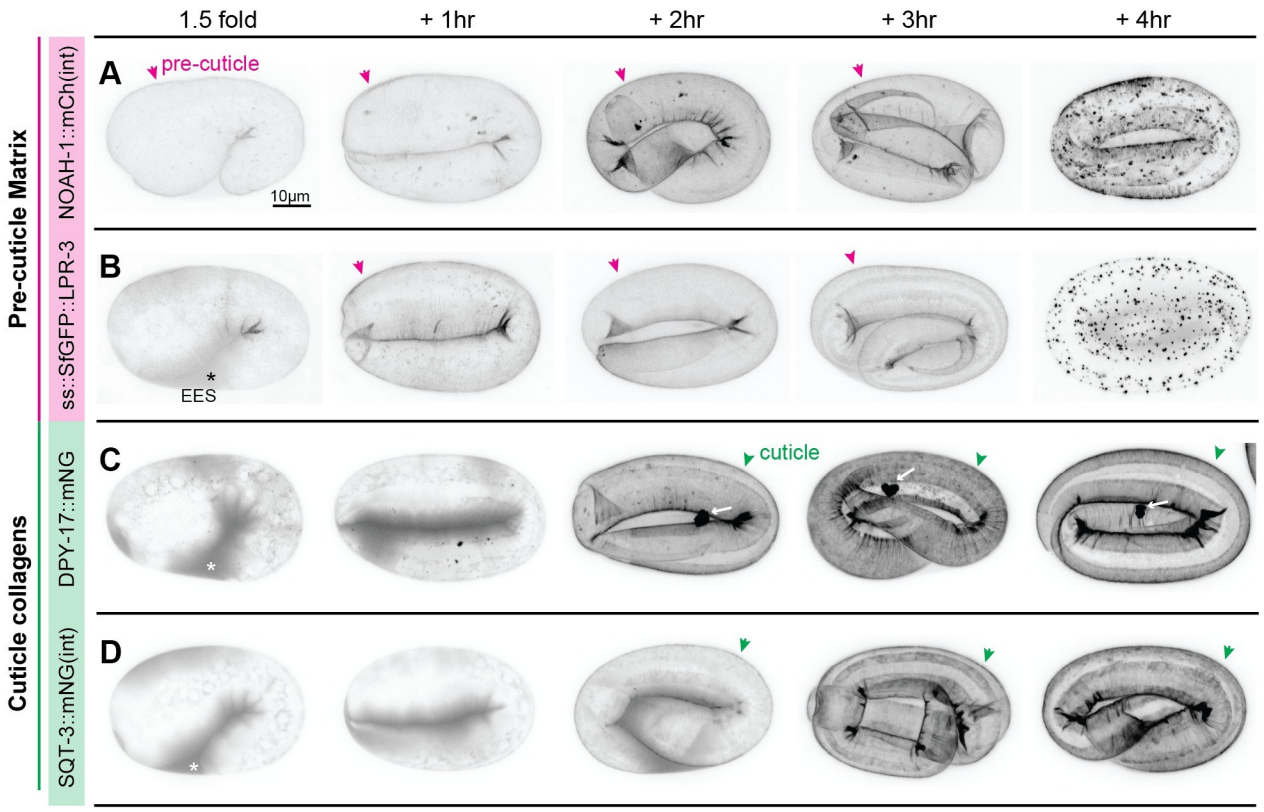

Fig 1. Matrix dynamics during assembly of the first pre-cuticle and cuticle. *C. elegans* embryos expressing functional pre-cuticle (A-B) or cuticle collagen (C-D) fusion proteins from endogenously-tagged loci. A) *noah-1(mc68* [NOAH-1::mCherry(int)]). B) *lpr-3(cs250* [ss::SfGFP::LPR-3]). C) *dpy-17(syb3685* [DPY-17::mNG]). D) *sqt-3(syb3691* [SQT-3::mNG(int)]). Embryos were selected at the 1.5-fold stage and then incubated for the indicated number of hours prior to imaging. Magenta arrowheads indicate pre-cuticle sheath. Green arrowheads indicate cuticle and white arrows indicate extracellular DPY-17::mNG aggregates. Asterisks indicate secreted fusion protein within the extraembryonic space (EES). All images are maximum intensity projections from confocal Z-slices, shown in inverted grayscale for clarity. Images are representative of at least n = 5 embryos per genotype per stage for A and B, and n = 10 embryos per genotype per stage for C and D. Scale bar, 10 microns.

https://doi.org/10.1371/journal.pgen.1010944.g001

Images were collected at the 1.5-fold stage and then at one-hour intervals thereafter, as the embryos elongated to their ultimate worm body shape.

The pre-cuticle or "sheath" matrix can be detected by the 1.5-fold stage and is important for proper embryo elongation beyond the 2-fold stage [28,32,58]. Consistent with that, the pre-cuticle ZP protein NOAH-1 tightly marked the pre-cuticle from before 1.5-fold to post-elongation (Fig 1A), as previously reported [32]. The secreted lipocalin LPR-3 initially accumulated between the embryo and the eggshell, and then marked pre-cuticle beginning about an hour after NOAH-1 (Fig 1B). Both proteins then were endocytosed and cleared. mCherry fusions but not Superfolder (Sf) GFP fusions accumulated in large lysosome-like structures (S1 Fig), suggesting that endocytosed protein eventually moved into an acidic endolysosomal compartment where acid-tolerant mCherry fusions (or cleaved mCherry) can continue to fluoresce but SfGFP fusions are quenched [59]. Together these data indicate that pre-cuticle matrix assembly occurs in a stepwise fashion. Furthermore, pre-cuticle matrix clearance involves considerable endocytosis.

Assembly of the first cuticle traditionally has been thought to begin late in embryogenesis, about 4 hours after 1.5-fold [58,60]. However, we found that tagged cuticle collagens DPY-17 and SQT-3 were secreted before the 1.5-fold stage, contemporaneously with pre-cuticle factors (Fig 1C and 1D). These collagens initially accumulated between the embryo and the eggshell,

began to incorporate detectably into matrix by the 2-hour timepoint (when embryos had elongated to the 3-fold stage), and appeared fully incorporated by the 3-to-4-hour timepoints. DPY-17 also consistently marked a single large extracellular aggregate that appeared in the extracellular space concomitant with matrix incorporation, consistent with some change in its molecular properties at this time (Fig 1C). In summary, the transition from pre-cuticle to cuticle begins during embryo elongation and components of both types of matrices transiently coexist, with the pre-cuticle disassembling once embryo elongation is complete. Furthermore, collagen secretion occurs earlier than previously thought, yet detectable collagen matrix incorporation occurs 2–3 hours afterwards, consistent with post-transcriptional (and possibly post-secretory) controls of cuticle matrix assembly.

BLI-4 is widely expressed in external epithelia and localizes to intracellular compartments and the extraembryonic space

The PCSK BLI-4 is a strong candidate for cleaving cuticle collagens to promote matrix assembly [25,47]. Existing single cell RNA sequencing (scRNAseq) data from embryos [52] revealed *bli-4* expression in external epithelial cells (e.g. those lined by pre-cuticle/cuticle), including the epidermis and various interfacial tubes and glia, as well as in the foregut (pharynx), intestine, and germline (S2 Fig). Consistent with this, a *bli-4* transcriptional reporter [61] also showed widespread epithelial expression, including in both the lateral (seam) and major (hyp7) epidermis and in the excretory duct and pore tubes (Fig 2A). A functional BLI-4::SfGFP(int) fusion protein, tagged at the protease domain and expressed from the endogenous locus, marked sub-apical intracellular compartments of external epithelia at the 1.5-fold stage and beyond (Fig 2B). BLI-4::SfGFP(int) also was faintly visible in the extraembryonic space (Fig 2B) and it appeared transiently within the lumen of the foregut at the 1.5+4 hr timepoint (Fig 2C). In summary, BLI-4 is expressed in external epithelia before and during cuticle assembly, and it appears both intracellular and extracellular.

Generation of *bli-4* null and isoform-specific mutants

The *bli-4* gene has many splice isoforms that differ in their 3' exons; the resulting proteins all share the N-terminal peptidase domain but differ in the presence or absence of other domains (Fig 3A and 3B) [47]. These isoforms may have different substrate specificities. For example, *bli-4(e937)* (hereafter *bli-4(ΔBLI))* is a deletion removing exons unique to isoforms a, e, g, and h as well as part of the 3'UTR of isoform f and intronic sequences of the other remaining isoforms; these mutants are viable but have a blistered (Bli) adult cuticle, suggesting failure to process key substrates unique to that stage [47]. BLI-4 isoforms c and d contain a cysteine-rich domain (CRD) similar to that found in mammalian furin, PCSK5, and PCSK6 (Fig 3A). The PCSK5 CRD can confer cell surface anchoring via binding to heparan sulfate proteoglycans [49,50], and was therefore proposed to affect substrate specificity. Based on an analysis of 3' end reads from embryo scRNAseq data [52], the *bli-4a*, *d* and *f/g* isoforms are detectably expressed in the embryo. *bli-4d* is by far the most highly expressed isoform in the embryonic epidermis and is also detected at lower levels in other tissues such as glial and excretory cells, the pharynx and intestine, and the germline (S2 Fig). Isoform *bli-4a* is expressed primarily in the germline and isoforms f/g are expressed most strongly in pharyngeal epithelial cells, though both are also detected in epidermis to a lesser degree (S2 Fig). The predicted sizes of these BLI-4 isoforms are consistent with the most prominent bands observed on Western blots of lysates from BLI-4::SfGFP(int)-expressing embryos (Fig 3C and 3D).

To address the overall roles of BLI-4, and roles of the two CRD-containing isoforms specifically, we used CRISPR/Cas9 to generate new *bli-4* null and isoform-specific alleles in an

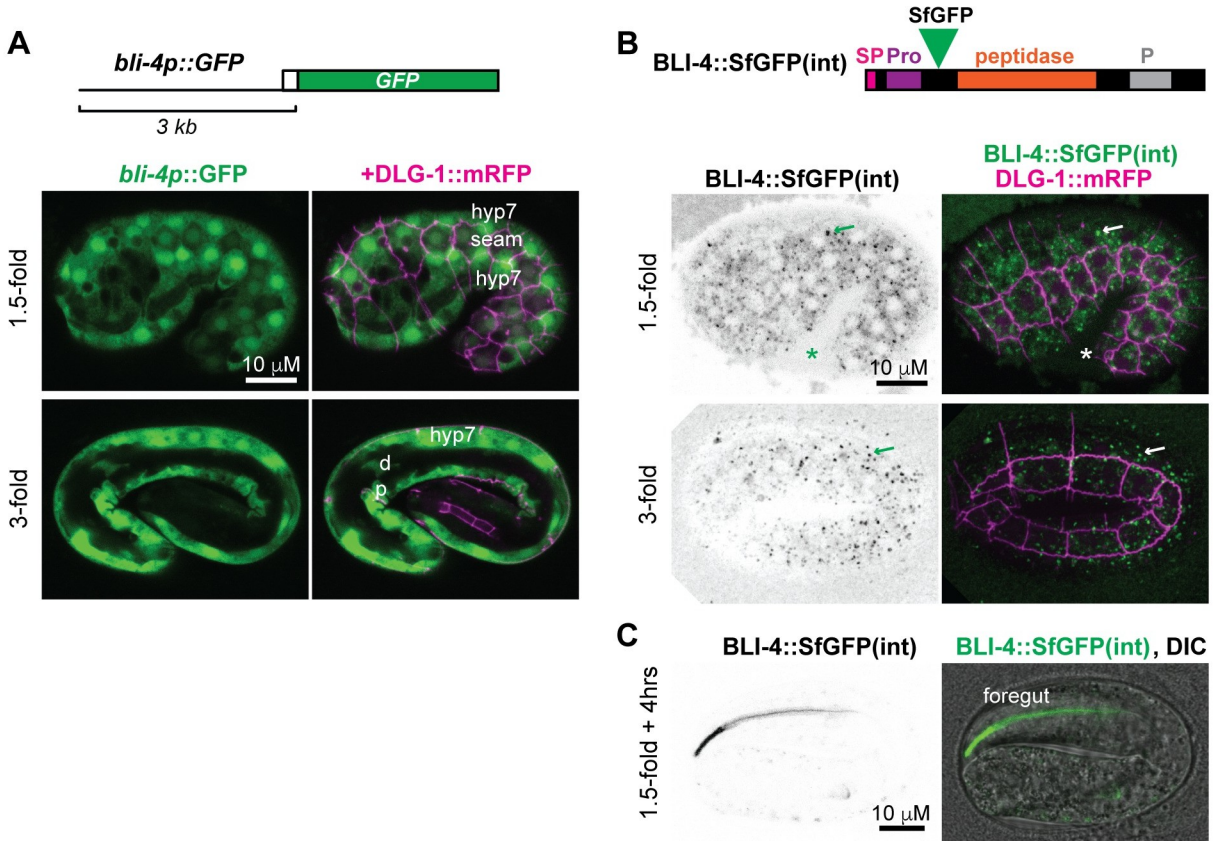

Fig 2. BLI-4 localizes to intracellular and extracellular compartments. A,B,C) Transcriptional and translational reporters reveal *bli-4* expression throughout pre-cuticle and cuticle assembly. Animals also express the epithelial junction marker DLG-1::RFP (*mcIs46*, magenta) to aid in cell identification and Z-depth assessment. Images are maximum intensity projections from confocal Z-stacks and representative of at least n = 8 animals examined per genotype per stage. A) A *bli-4pro*::*GFP* transcriptional reporter (*sEx11763*, green) [61] is broadly expressed in external epithelia, including in hyp7, seam cells, and in the excretory duct (d) and pore (p). B) An endogenous BLI-4::SfGFP(int) translational fusion (*syb5321*) marks intracellular puncta within epithelia and is faintly detectable within the extraembryonic space (EES). Single channel images are shown in inverted grayscale for clarity. Asterisk, fusion protein detected in the extraembryonic space. Arrow, intracellular puncta. CRISPR/Cas9 was used to insert SfGFP between the BLI-4 prodomain (Pro) and peptidase domain, as indicated (S2 Table). The schematic shows the short isoform BLI-4f (Genbank NP_001360008.1), but all isoforms should be tagged. ss, signal sequence. P, P domain. C) BLI-4::SfGFP(int) transiently accumulated in the foregut at the 1.5 + 4hr timepoint.

https://doi.org/10.1371/journal.pgen.1010944.g002

isogenic strain background (Fig 3B, S2 Table and Methods). Two null alleles (*cs281* and *cs283*, hereafter *bli-4(-)*) were made by targeting exon 2, upstream of the peptidase domain; these cause frameshifts that should remove all splice isoforms. Two isoform c- & d-specific mutants (*cs302* and *cs308*, hereafter *bli-4(ΔCRD)*) and two isoform d-specific mutants (*cs293* and *cs295*) were made by targeting exons unique to those isoforms. All mutants were recessive lethal but could be rescued with a fosmid-based transgene containing the entire *bli-4* genomic locus (Figs 3E, 4 and 5). *bli-4(-)* failed to complement the isoform-specific alleles, as expected, whereas *bli-4(ΔCRD)* and *bli-4(ΔBLI)*, which remove distinct sets of isoforms, complemented each other (Figs 3E and 4B).

bli-4 null mutants arrest as retracted embryos following elongation

bli-4(-) mutants were embryonic lethal (Emb), as previously reported for other null alleles (Fig 4A and 4C) [47]. Mutant embryos arrested as disorganized masses with occasional excretory tube dilations and evidence of debris between the embryo and the eggshell (Fig 4A). Although

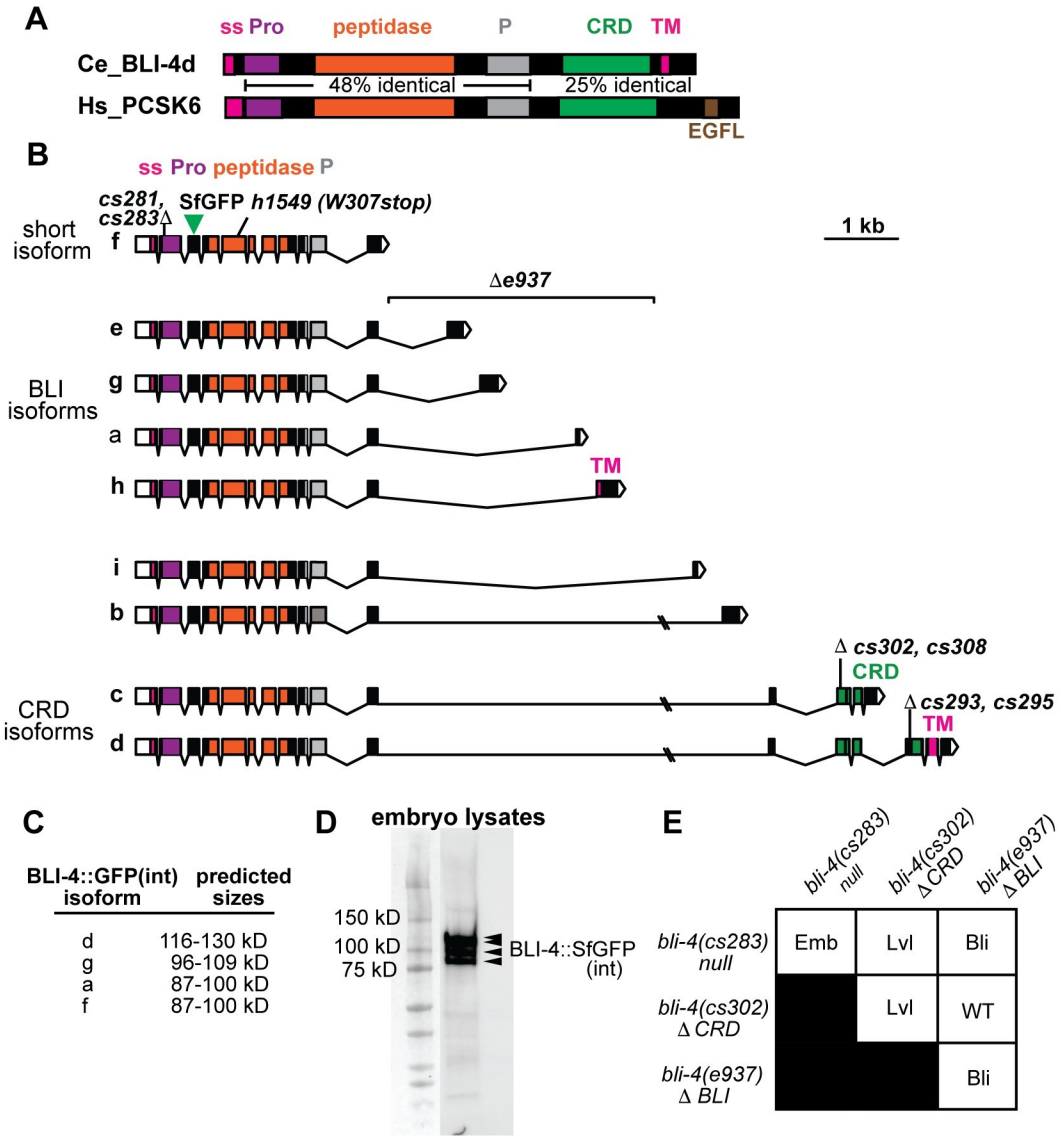

Fig 3. Generation of *bli-4* null and isoform-specific alleles. A) *C. elegans* BLI-4d (Genbank NP_001021543.1) protein schematic and comparison to human PCSK6 (Genbank BAA21625.1). The % identity at the amino acid level is listed between relevant domains. Like other PCSK family members, both proteins have a signal peptide (SP) and prodomain (Pro) that are removed during trafficking, followed by the peptidase domain and an associated P domain thought to assist with its folding and stability [48]. BLI-4d and PCSK6 also share a cysteine-rich domain (CRD). BLI-4d also has a transmembrane (TM) domain but it lacks the EGF-like (EGFL) domain found in PCSK6. B) *bli-4* gene isoforms and mutant alleles. Colors indicate encoded protein domains, as in A. Isoforms are arranged by mutant groups. *cs281* and *cs283* are 1-2nt deletion/frameshift mutations in exon 2, which is shared among all *bli-4* isoforms. *e937* is a 3,325 bp deletion that removes intronic sequences and exons associated with isoforms a, e, g, and h [47]. *cs302* and *cs308* are 4–19 nt indel/frameshift mutations in the first exon unique to isoforms c and d. *cs293* and *cs295* are identical 5nt deletion/frameshift mutations in the first exon unique to isoform d. See S2 Table for specific allele sequences. C) Predicted sizes of major embryonically-expressed BLI-4::SfGFP(int) fusion proteins before and after removal of the Pro domain. Sizes were estimated based on the isoform sequence using https://www.bioinformatics.org/sms/prot_mw.html. See also S2 Fig for data regarding isoform expression in the embryo. D) Western blot of lysates from BLI-4::SfGFP(int) expressing embryos. Arrowheads indicate four major bands between 80 and 130 kD. Blot is representative of 3 replicates. E) Summary of complementation test results. *bli-4(cs281)* failed to complement both *bli-4(cs302)* (n = 59) and *bli-4(e937)* (n = 120) for the larval lethal (Lvl) and adult Blister (Bli) phenotypes, respectively, while *bli-4(cs302)* complemented *bli-4(e937)* (n = 186). Balancer *hT2 [bli-4(e937) let-?(q782) qIs48] (I;III)* was used as the *bli-4(e937)*-containing chromosome.

https://doi.org/10.1371/journal.pgen.1010944.g003

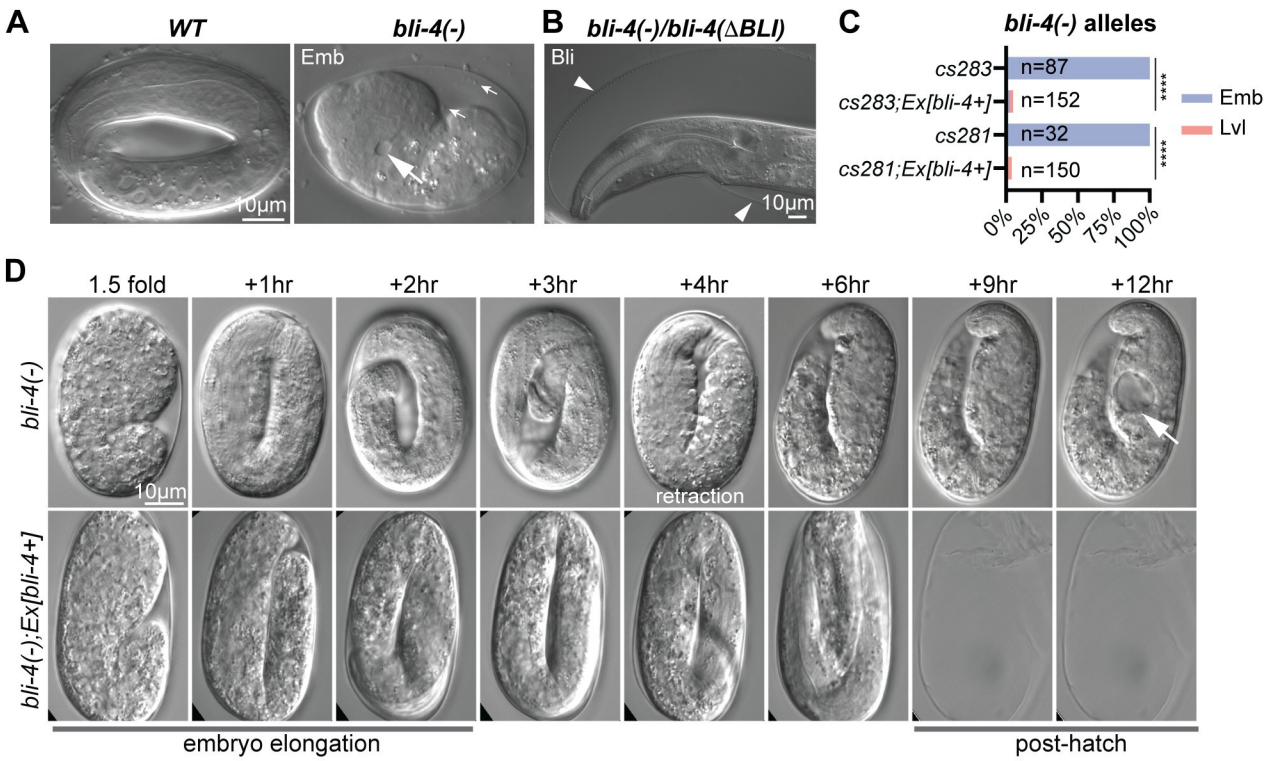

Fig 4. *bli-4* null mutants retract and collapse after embryonic elongation. A) In contrast to a wildtype 3-fold embryo (left), *bli-4*(-) embryos arrest as misshapen masses with excretory tube dilations (large arrows) and extracellular debris (small arrows). B) *bli-4(-)* allele *cs283* failed to complement *bli-4(e937)* for the adult Blister (Bli) phenotype (n = 120). Balancer *hT2 [bli-4(e937) let-?(q782) qIs48] (I;III)* was used as the *bli-4(e937)*-containing chromosome. Arrowheads point to blistered cuticle. C) Phenotype quantitation and rescue of *bli-4(-)* mutants. *Ex(bli-4+)* corresponds to transgene *csEx919*, which contains fosmid WRM069bE05. ***P<0.0001, Fisher's Exact Test. D) Stills from time-lapse imaging of *bli-4(cs281)* and rescued siblings at 12˚C. *bli-4(-)* embryos initially elongated but then began retracting after the 3-hour timepoint (220–330 minutes, n = 5). Arrow indicates excretory tube dilation. Note that the rescued embryo has an elongated eggshell shape, likely caused by pressure from the coverslip; however, this did not interfere with development and hatching.

https://doi.org/10.1371/journal.pgen.1010944.g004

the arrested embryos appeared unelongated, timelapse imaging revealed that mutant embryos did elongate initially, but then retracted and collapsed soon afterwards, about 4 hours after the 1.5-fold stage (Fig 4D and S1 and S2 Video). Notably, retraction occurred near the time when the cuticle replaces the pre-cuticle (Fig 1) and specifically resembled that previously reported for mutants lacking the essential cuticle collagen SQT-3 [58].

bli-4(ΔCRD) mutants arrest as Dumpy larvae with abnormal cuticles

The four *bli-4(ΔCRD)* or *bli-4(d)* mutants all appeared less severe than the null but similar to each other, with variable larval arrest (Lvl) at the L1, L2, or L3 stage (Fig 5A). Despite the accumulation of debris during embryogenesis (Fig 5B), the majority of these mutants elongated and hatched (Fig 5A). Mutants appeared only mildly Dumpy (Dpy) as L1 larvae, but they completely lacked the alae ridges typical of the L1 cuticle (Fig 5C). The L1 cuticle retained its barrier function to exclude Hoechst dye, but the gut permeability barrier appeared defective (Fig 5D), suggesting that one or more components of that barrier could be substrates for gut-expressed BLI-4d. *bli-4(ΔCRD)* mutants became more severely Dpy by the time of L2 or L3 arrest (Fig 5A), suggesting that the CRD isoforms are particularly important for processing substrates during the early larval stages. This strong Dpy phenotype resembles that of many cuticle collagen mutants [26,62,63].

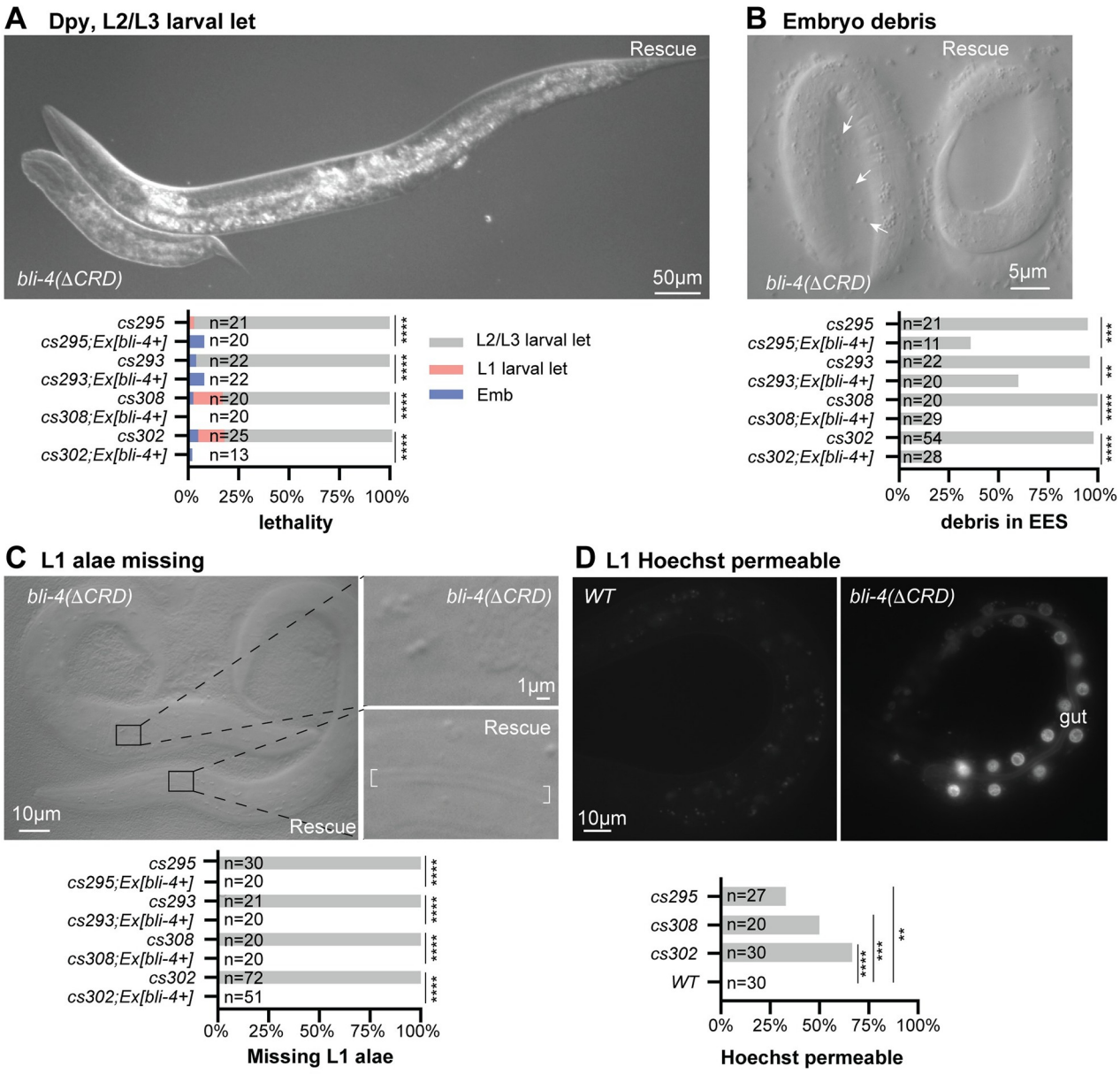

Fig 5. *bli-4* CRD isoform mutants arrest as Dumpy larvae with cuticle defects. A-D) *bli-4(ΔCRD)* isoform mutant phenotypes. Only images of *bli-4(cs302)* and rescued siblings are shown. Phenotype quantitation and rescue data for all alleles are shown below. The *bli-4+* rescue transgene is *csEx919*. *P<0.01, **P<0.001, ***P<0.0001, Fisher's Exact test. A) Most mutants arrest as Dumpy L2 or L3 larvae. Larvae in image are 48hr after egg lay (AEL). B) Embryos accumulate extracellular debris (small arrows) between the embryo and the eggshell. Embryos are 1.5 fold + 3–4 hours old. C) L1 larvae are slightly Dumpy and entirely lack cuticle alae ridges. Bracket indicates position of alae in the rescued sibling. D) Whereas *wild-type* L1 larvae have a permeability barrier that excludes Hoechst dye (left), many *bli-4(ΔCRD)* mutants had strong staining in the gut epithelium. Staining was not apparent in the epidermis or pharynx, suggesting a gut-specific barrier defect. Note that *bli-4d* is expressed in each tissue (S2 Fig) but likely has different substrates in each location since these tissues vary widely in their aECM composition.

https://doi.org/10.1371/journal.pgen.1010944.g005

BLI-4 promotes secretion and cuticle incorporation of collagens SQT-3 and DPY-17

Next, we examined our matrix fusions in *bli-4* mutant backgrounds. Although many ZP proteins are cleaved at a C-terminal CFCS site before matrix incorporation [2], we did not note any obvious change in the pre-cuticle appearance of a NOAH-1 fusion between wild type and

bli-4 mutants (S3 Fig). Therefore, protein trafficking was not generally disrupted. However, we did find significant differences in the appearance of both cuticle collagens (Figs 6 and 7).

SQT-3 is a predicted Type II transmembrane collagen with a cytosolic N-terminus and external C-terminus, plus a CFCS whose cleavage could release that collagenous C-terminus into the environment (Fig 6A). DPY-17 is a secreted collagen with an N-terminal CFCS (Fig 7A). Quite dramatically, in *bli-4(-)* mutants, both SQT-3::mNG(int) and DPY-17::mNG were poorly secreted and failed to accumulate robustly in the extra-embryonic space or to incorporate efficiently into the cuticle (Figs 6B, 6C, 6E and 7B, 7C, 7E). Instead, both collagens formed large puncta at or near the apical plasma membrane, with most puncta appearing at least partly intracellular when compared to the cuticle surface or an mCherry::PH membrane marker (Figs 6D–6H and 7D and 7E). Puncta were visible by the 1.5-fold stage (Figs 6B and 7B), several hours before normal matrix incorporation (Fig 1C and 1D). These data indicate that BLI-4 promotes initial secretion of the soluble forms of these two collagens.

bli-4(ΔCRD) mutants had less severe defects in collagen secretion; SQT-3 and DPY-17 fusions still formed some intracellular puncta, but they were at least partly secreted and eventually incorporated into the cuticle (Figs 6B–6E and 7B–7E). SQT-3 is the only known cuticle collagen required for *C. elegans* embryo viability, being critical to maintain embryo shape after elongation [27,58]; its partial secretion and incorporation in *bli-4(ΔCRD)* mutants but not *bli-4(-)* mutants likely contributes to the different arrest points of these mutants. These data are consistent with a role for multiple BLI-4 isoforms in cleavage of these collagens.

SQT-3 and DPY-17 are mutually dependent on each other for secretion

Although *dpy-17* null mutants have a less severe Dpy phenotype than *sqt-3* null mutants, prior data suggested that DPY-17 and SQT-3 function together and that DPY-17 is required for efficient SQT-3 secretion [45,64]. We were able to confirm this result; in *dpy-17(-)* mutants, SQT-3 accumulated cytosolically and in a halo pattern surrounding epidermal nuclei (Fig 8A and 8C), suggesting retention in the endoplasmic reticulum. Conversely, we found that SQT-3 is required for both DPY-17 secretion and overall protein accumulation; DPY-17 was barely detectable in *sqt-3(-)* mutants (Fig 8B and 8C). While the underlying mechanism remains to be investigated, decreases in protein stability are often observed after removal of a key binding partner [65]. Our data support the model that DPY-17 and SQT-3 travel together through the secretory pathway and suggest that *bli-4* loss could affect DPY-17 and SQT-3 both directly and indirectly via effects on the other (Fig 8D).

CFCS mutations in SQT-3 and DPY-17 mimic loss of *bli-4*

The dramatic aECM defects described above are consistent with roles for BLI-4 in the N-terminal processing of multiple cuticle collagens. Unfortunately, because *bli-4* mutants are lethal, it is difficult to collect large numbers of mutant embryos and we have not found appropriate *bli-4* knockdown and Western blot conditions to directly test if BLI-4 is required for collagen cleavage. Instead, we used CRISPR/Cas9 to mutate the predicted BLI-4-dependent cleavage sites from RxxR to AxxA within the endogenous SQT-3::mNG(int) and DPY-17::mNG fusions (see Figs 6 and 7). These CFCS mutations mimicked loss of *bli-4*, causing intracellular retention of the mutant proteins (Fig 9A–9D). Some mutant collagen eventually incorporated into the L1 cuticle, but matrix structures appeared abnormal and larvae exhibited a severe Dpy phenotype (Fig 9E and 9F). Because most *sqt-3* and *dpy-17* CFCS mutants survive past hatch, unlike *bli-4(-)* mutants, the embryonic arrest phenotype of *bli-4(-)* likely reflects cumulative effects on multiple substrates. Nevertheless, these data strongly support the model that BLI-4 directly cleaves both SQT-3 and DPY-17 collagens to promote their secretion.

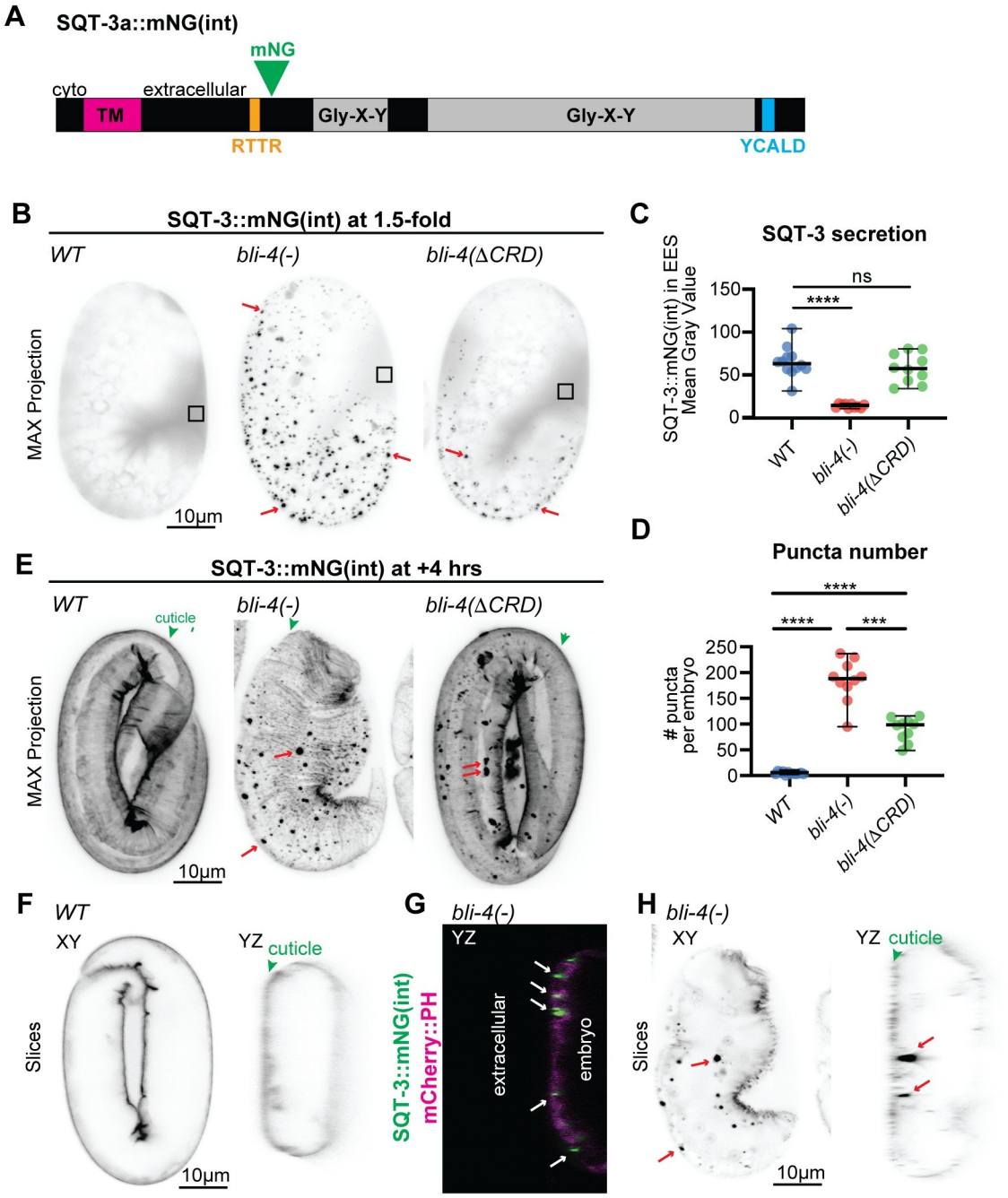

Fig 6. BLI-4 promotes secretion of SQT-3 cuticle collagen. A) Schematic diagram of the SQT-3::mNG(int) fusion, showing Gly-X-Y collagen domains (gray) and N-terminal CFCS (RTTR, orange). SQT-3 lacks a signal peptide but contains a predicted transmembrane (TM) domain (magenta). A predicted DPY-31-dependent cleavage site (blue) near the C-terminus is also shown. B) SQT-3::mNG(int) is poorly secreted and accumulates in puncta in *bli-4* null mutants. Maximum intensity projections of 1.5-fold embryos expressing SQT-3::mNG. Box indicates extra-embryonic region analyzed in C. Images shown are representative of at least n = 10 images per genotype. C,D) Quantitation of SQT-3::mNG(int) signal in the extraembryonic space (EES) (C) or of puncta number (D) in *WT* vs. *bli-4* 1.5-fold embryos. ***, P<0.001, ****, P<0.0001, Mann-Whitney U test. E) Maximum intensity projections from confocal Z-stacks of embryos at the 1.5-fold + 4-hour stage. By this stage *bli-4* null mutants collapsed with minimal SQT-3::mNG(int) matrix incorporation, whereas *bli-4(cs302)* mutants showed significant incorporation into the cuticle (green arrowhead). Images shown are representative of at least n = 10 embryos per genotype. F-H) Orthogonal views of *WT* (F) and *bli-4 (cs281)* (G, H) embryos expressing SQT-3::mNG(int). Embryo in (G) also contains a membrane marker *let-653pro*::mCherry::PH (*csIs98*). Aggregates (arrows) appear to be intracellular or to span the plasma membrane. *bli-4* embryo in (H) is the same as that shown in (E).

https://doi.org/10.1371/journal.pgen.1010944.g006

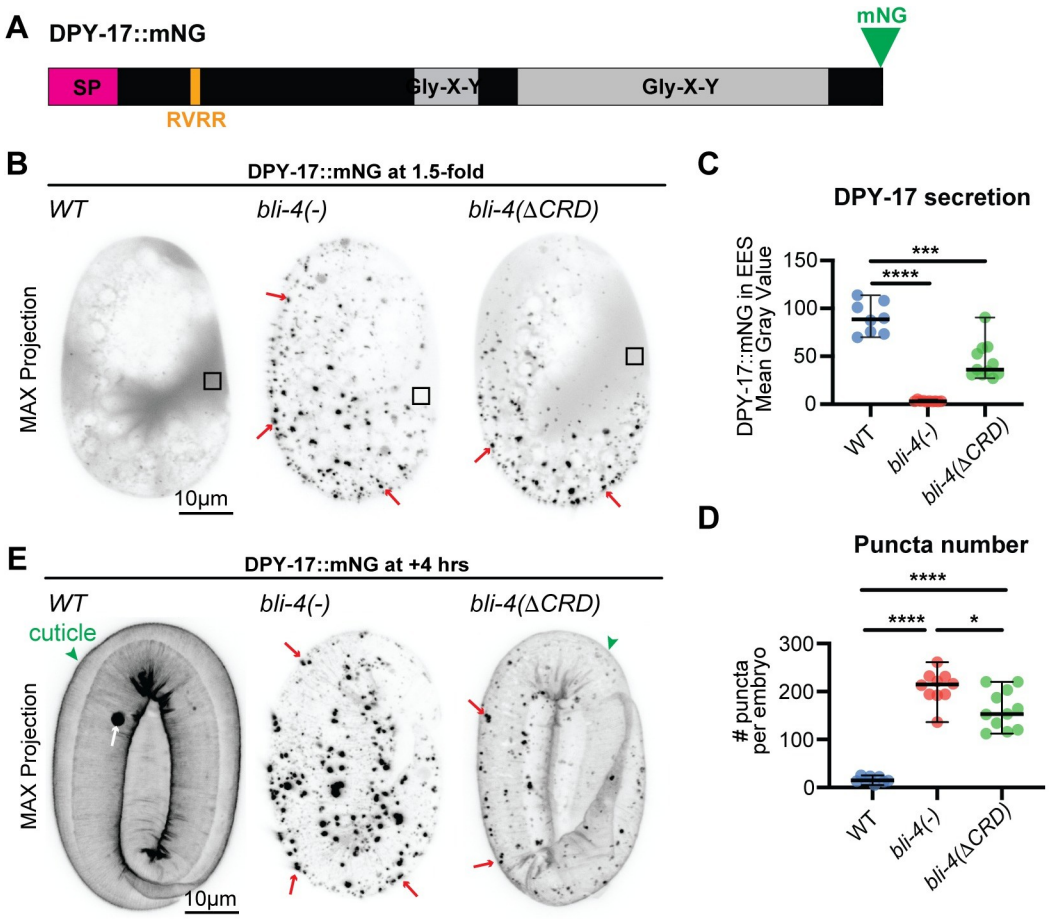

Fig 7. BLI-4 promotes secretion of DPY-17 cuticle collagen. A) Schematic diagram of the DPY-17::mNG fusion, showing Gly-X-Y collagen domains (gray), signal peptide (SP, magenta) and N-terminal CFCS (RVRR, orange). B) DPY-17::mNG is poorly secreted and accumulates in puncta in *bli-4* null mutants. Maximum intensity projections of 1.5-fold embryos expressing DPY-17::mNG. Box indicates extra-embryonic region analyzed in C. Images shown are representative of at least n = 8 images per genotype. C, D) Quantitation of DPY-17::mNG signal in the extraembryonic space (EES) (C) or of puncta number (D) in *WT* vs. *bli-4* 1.5-fold embryos. *, P = 0.012, ***, P<0.001,***P<0.0001, Mann-Whitney U test. E) Maximum intensity projections from confocal Z-stacks of embryos at the 1.5-fold + 4 hour stage. By this stage *bli-4* null mutants collapsed with minimal DPY-17::mNG matrix incorporation, whereas *bli-4(cs302)* mutants showed significant incorporation into the cuticle (green arrowhead). Images shown are representative of at least n = 9 embryos per genotype.

https://doi.org/10.1371/journal.pgen.1010944.g007

SQT-3 CFCS mutant puncta accumulate independently of DPY-31 astacin

DPY-31, a BMP1-related astacin protease, previously was proposed to cleave the SQT-3 C-terminus to promote matrix assembly [44–46]. We confirmed that, in *dpy-31* mutants, SQT-3 was still efficiently secreted but its cuticle incorporation was delayed compared to wild type (Fig 10A). However, SQT-3 eventually incorporated into the cuticle of *dpy-31* mutants (Fig 10B), suggesting either that C-terminal cleavage is not absolutely required or that other proteases can also execute this cleavage (Fig 10E). Furthermore, *dpy-31* loss did not significantly reduce the number or size of SQT-3 CFCS mutant puncta (Fig 10C and 10D); therefore, puncta accumulation is not due to premature cleavage by DPY-31. Instead, retention of the SQT-3 N-terminus may allow inappropriate interactions with other unknown factors along the secretory pathway, blocking release and/or leading to intracellular aggregation (Fig 10E).

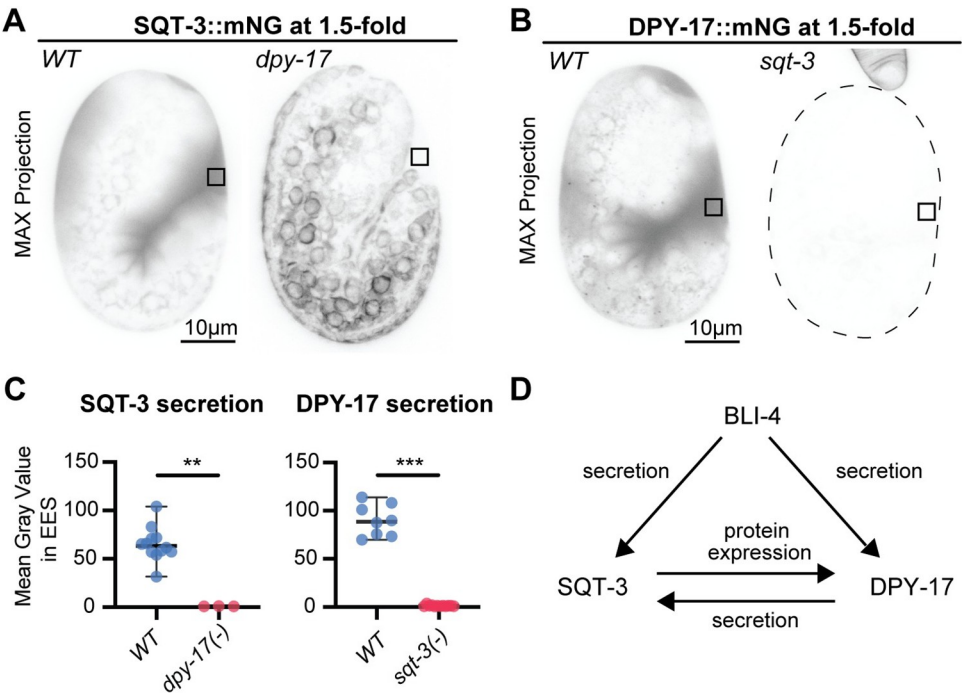

Fig 8. SQT-3 and DPY-17 collagens are mutually dependent for secretion. A) Maximum intensity projections of embryos expressing SQT-3::mNG. *dpy-17(e164)* mutant embryos retained most SQT-3::mNG intracellularly (n = 3). Similar results were observed in another n = 7 3-fold embryos and match those previously reported by immunostaining [45]. B) Maximum intensity projections of embryos expressing DPY-17::mNG. DPY-17::mNG was barely detectable in *sqt-3(e2924ts)* mutants, even at the permissive temperature of 15˚ C (n = 12). Similar results were obtained in another n = 15 3-fold embryos. C) Quantitation of fluorescence intensity in the extraembryonic space. **, P = 0.0044, ****, P<0.0001, Mann-Whitney U test.D) Model summarizing SQT-3 and DPY-17 relationship and possible direct and indirect effects of BLI-4 on each.

https://doi.org/10.1371/journal.pgen.1010944.g008

Discussion

N-terminal processing is an important step in the maturation of mammalian fibrillar collagens and is generally thought to affect fibril structure. Here we provide evidence for an alternative role of N-terminal processing in *C. elegans* cuticle collagens: to allow secretion of soluble forms of collagen prior to matrix assembly (Fig 10E). Using new collagen fusion knock-ins that allowed us to visualize *C. elegans* cuticle assembly in live embryos, we showed that collagen secretion into the extraembryonic space precedes cuticle assembly by several hours. Loss of *bli-4* PCSK prevents efficient secretion of two early cuticle collagens, SQT-3 and DPY-17, causing them to accumulate within apical compartments of epidermal cells and reducing (but not completely blocking) their later assembly into cuticle matrix. Mutation of the predicted BLI-4-dependent cleavage sites causes similar defects. These data demonstrate a role for collagen N-terminal processing in intracellular trafficking and control of matrix assembly *in vivo* and prompt a revision of the classic model for *C. elegans* cuticle matrix assembly and the pre-cuticle-to-cuticle transition.

Temporal control of cuticle assembly and the pre-cuticle to cuticle transition

The *C. elegans* pre-cuticle and cuticle are molecularly distinct matrices that coat external epithelia at different stages of development. The pre-cuticle is present at earlier stages and is required for initial embryo elongation, while the cuticle eventually replaces it and is

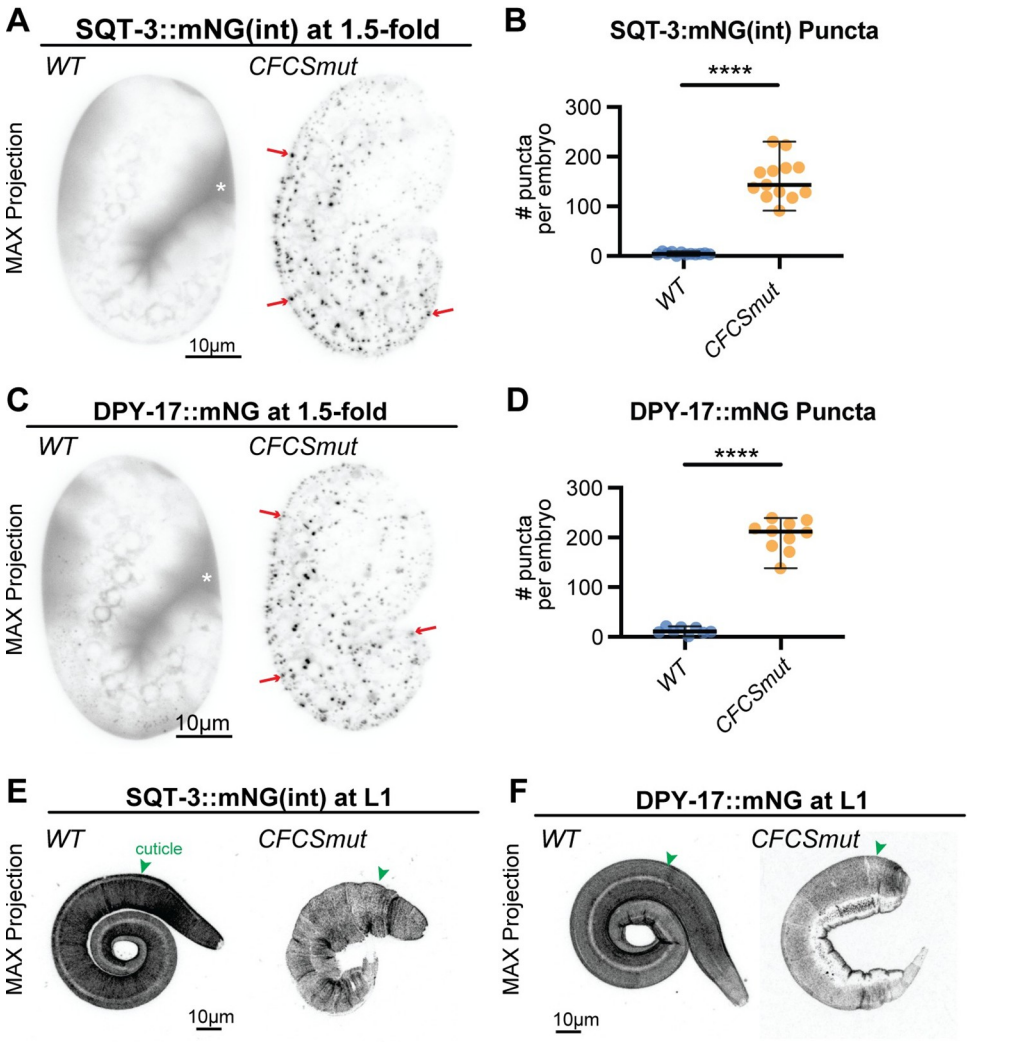

Fig 9. CFCS mutants for SQT-3 and DPY-17 form intracellular puncta. Maximum intensity projections and puncta quantifications of 1.5-fold embryos (A-D) or L1 larvae (E,F) expressing A,B,E) SQT-3::mNG(int) vs. SQT-3(R79A, R82A)::mNG(int)) and (C,D,F) DPY-17::mNG vs. DPY-17(R61A,R63A,R64A)::mNG. Although poorly secreted, the CFCS mutant collagens did eventually incorporate into cuticle. Images shown are representative of at least n = 10 animals per genotype per stage. At the plate level, 100% of mutant L1s showed a Dpy phenotype (n>1000 per strain). ****, p<0.0001, Mann-Whitney U test.

https://doi.org/10.1371/journal.pgen.1010944.g009

responsible for maintaining embryo shape [28,32,58]. Consistent with those defined roles, we showed here that the transition to cuticle matrix happens during and shortly following embryo elongation. Surprisingly, prior to this transition, at least some cuticle collagens are present in the extra-embryonic space for several hours without appearing to substantively aggregate or incorporate into matrix. Eventually, cuticle collagens gradually incorporate and then transiently co-exist in the matrix with pre-cuticle proteins. After the collagens have incorporated, pre-cuticle proteins are removed by endocytosis.

This sequence of events suggests a revision of the classic model for *C. elegans* cuticle assembly, in which sequentially-deposited distinct layers are pushed progressively further away from the plasma membrane [66,67]. The pre-cuticle does not become the outer layer of the mature cuticle. Furthermore, since cuticle collagen matrix assembly does not immediately follow secretion, it could potentially occur external to or within the initial pre-cuticle layer rather

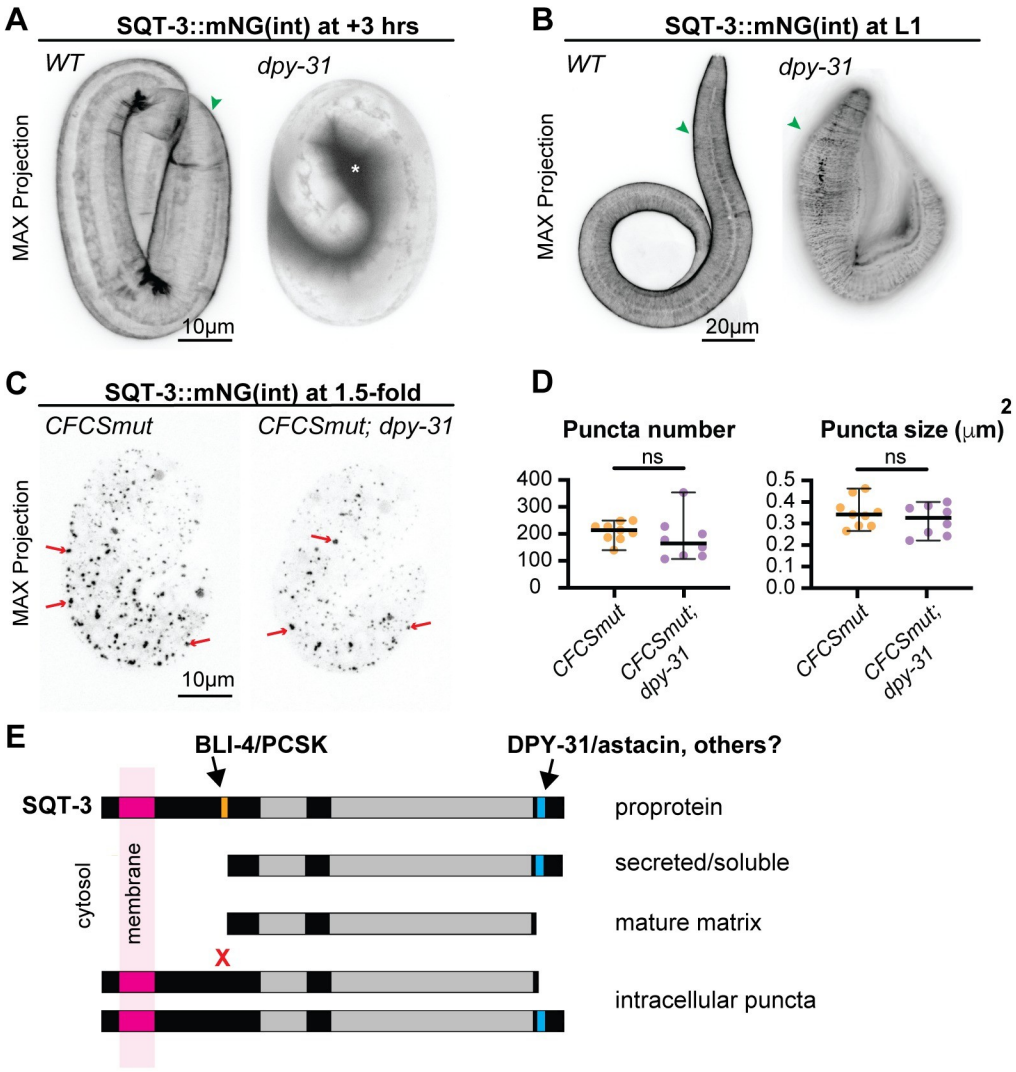

Fig 10. SQT-3 CFCS mutant puncta form independently of DPY-31/astacin. A-C) Maximum intensity projections of WT vs. *dpy-31(e2770)* mutants expressing A,B) SQT-3::mNG(int) or C) CFCS mutant SQT-3(R79A,R82A)::mNG (int)). D) Quantification of puncta number and size in embryos from C. DPY-31 promotes timely SQT-3 matrix incorporation (A) and proper cuticle structure (B), but its removal does not suppress the SQT-3 CFCS aggregation defect (C,D). Images shown are representative of at least n = 8 animals per genotype. E) Model for sequential cleavage of SQT-3 collagen by BLI-4/PCSK and DPY-31/astacin. BLI-4 promotes secretion of soluble forms of SQT-3, while DPY-31 and possibly other astacin proteases promote mature matrix assembly. Preventing BLI-4-dependent N-terminal cleavage (X) leads to intracellular retention. This occurs independently of DPY-31, but could reflect premature matrix assembly due to inappropriate modification by other assembly-promoting factors such as other astacin proteases, proline hydroxylases [86], or tyrosine cross-linking enzymes [72,73].

https://doi.org/10.1371/journal.pgen.1010944.g010

than more membrane-proximally. This means that the earliest expressed collagens need not necessarily join the matrix first nor ultimately define more external cuticle layers. For example, despite the early SQT-3 secretion shown here, *sqt-3* mutants are defective in formation of the basal striated layer of the L1 cuticle, which forms only after embryo elongation [58]. We propose that the layered organization of the final cuticle structure is determined not only by the initial timing of cuticle collagen expression and extracellular release, but also by processing events and protein-protein interactions that occur in the extracellular environment or along the still poorly understood routes that these collagens take through the secretory pathway.

We do not currently know if the early pool of secreted collagen has a function or if the collagen that joins the cuticle comes from that extracellular pool (an "outside in" assembly direction) or from a later wave of secreted protein (an "inside out" assembly direction). A very interesting recent study suggested that mammalian fibrillar collagens are initially secreted in soluble form and then re-endocytosed and recycled through a distinct secretory pathway before being competent for fibril elongation [68]. Our observations could be consistent with such a model and set the stage for more detailed future studies of collagen trafficking and matrix assembly in the *C. elegans* system.

Further studies also will be needed to determine if subsequent rounds of new cuticle assembly in *C. elegans* larvae follow the same early secretory schedule as in the embryo. The embryo is surrounded by a relatively impermeable eggshell that keeps secreted proteins concentrated near the plasma membrane and therefore potentially available for later assembly. The old cuticle could serve a similar role in larvae. However, it is also possible that transcriptional regulators of oscillatory gene expression take on a larger role in the post-embryonic stages.

Transmembrane and secreted collagens function together to form the cuticle

Sequence predictions suggest that only about a third (56/173) of *C. elegans* cuticle collagens are secreted using a conventional N-terminal signal sequence (as for DPY-17), while the remainder (like SQT-3) are predicted to be secreted in type II orientation with a cytosolic N-terminus followed by a transmembrane domain [27]. Like mammalian MACITs and other collagen-related transmembrane proteins [16,17], these transmembrane cuticle collagens could potentially remain associated with cell surfaces or could be released to the environment by proteolysis. Our observations indicate that a substantial portion of SQT-3::mNG(int) is released from the cell surface at early timepoints, but it is possible that a later switch to membrane retention is one mechanism that helps initiate cuticle assembly.

Our imaging of DPY-17 and SQT-3 fusions also confirm and extend prior evidence that these two very different collagens rely on each other for trafficking through the secretory pathway [45]. In the absence of DPY-17, SQT-3::mNG(int) appears stuck in the ER, while in the absence of SQT-3, DPY-17::mNG is barely detectable. A similar reduction in levels of another cuticle collagen, DPY-7, were reported after removal of collagens that co-localize with it in cuticle furrows [69], suggesting that many functionally-related collagens may require each other for trafficking and/or stability. It will be interesting to investigate if such dependencies reflect the existence of heteromeric collagen triple helices or some other higher order matrix structures that begin to assemble intracellularly.

Roles for N-terminal and C-terminal processing in *C. elegans* cuticle collagen secretion and matrix assembly

C. elegans cuticle collagens resemble mammalian transmembrane collagens in having predicted N-terminal cleavage sites that match the consensus for furin/PCSKs rather than ADAMTS proteinases [13,14]. A recent bioinformatic analysis found that 109 of the 173 predicted cuticle collagens contain an N-terminal CFCS that specifically matches the sequence RxxR [27]. An RxxR sequence was found in most cuticle collagens with predicted secretion signal sequences (45/56) and in more than half of the predicted transmembrane cuticle collagens (64/117). N-terminal cleavage at CFCS sites is important for function of multiple collagens, since mutations in these sites cause cuticle abnormalities [13,14,25] (this work). BLI-4 previously was speculated to be the PCSK that performs these N-terminal cleavages [25,47] and our data strongly support that model for the two collagens tested here, SQT-3 and DPY-17.

Surprisingly, loss of BLI-4 or mutation of its predicted collagen target sites caused a substantial portion of SQT-3 and DPY-17 to accumulate within an apical compartment rather than being released in soluble form to the external environment. This defect cannot be attributed simply to failure to release a transmembrane form of SQT-3 collagen, since a CFCS mutation in DPY-17 (a secreted collagen) also caused retention within intracellular puncta. Our interpretation of these apical puncta is that they correspond to a secretory compartment from which collagens can't be released without N-terminal cleavage. Another possible (not mutually exclusive) interpretation is that they correspond to insoluble aggregates that form as the unprocessed procollagens move through the secretory pathway and encounter other partners or environments that allow them to initiate matrix assembly prematurely (Fig 10E). This latter model implies that N-terminal processing of SQT-3 and DPY-17 inhibits a key step of matrix assembly during trafficking, in contrast to the more typical scenario where proprotein cleavage facilitates matrix assembly.

In humans, failure to remove the Type I procollagen N-terminus leads to Ehlers-Danos syndrome type VII, a matrix disorder characterized by frequent joint dislocations and tissue fragility [4,9,11]. In that case, the collagen molecules that retain their N-termini incorporate into abnormal fibrils, but to our knowledge no defects in secretion or in the timing of fibril formation have been reported [21,22]. Part of this difference could be technical based on the *in vivo* imaging vs. *in vitro* biochemical approaches used, but it is also clear that there are many biological differences in collagen regulation between different families of collagens. Indeed, in mammalian fibrillar collagens, triple helix formation initiates at the C-terminus and then proceeds towards the N-terminus, whereas in MACIT collagens the opposite is true [15,70]. The direction of triple helix assembly is not known for *C. elegans* cuticle collagens, but it has been noted that some have N-terminal coiled-coil regions that could serve as oligomerization domains [71]. *C. elegans* and mammalian collagens also differ in other processing events, for example *C. elegans* cuticle collagens display tyrosine-based crosslinking rather than hydroxylysine based crosslinking [72,73]. It is not unreasonable to hypothesize that N-terminal cleavage may serve different roles in such different contexts.

Our data also suggest that the role of C-terminal cleavage could vary among cuticle collagen subtypes. Although SQT-3 contains a predicted BMP1/astacin cleavage site and requires DPY-31 for timely matrix assembly [44,45] (this work), we note that many other cuticle collagens, including DPY-17, do not have recognizable sites for C-terminal processing. Furthermore, C-terminal tags are retained on DPY-17 and multiple other cuticle collagens in matrix structures [63,74], suggesting that those collagens may not undergo such processing. Instead, there may be other unknown modifications, partners, and/or environmental conditions that must be present in order for those collagens to initiate matrix assembly.

Intracellular vs. extracellular processing of collagens

Despite the clinical importance of Type I procollagen processing, there is still debate in the literature about when and where this happens. C-terminal procollagen cleavage is thought to occur in a late secretory compartment or at the plasma membrane, while N-terminal cleavage may occur either before or after that [3,7]. Growing evidence suggests N-terminal processing occurs at least in part within an ER or Golgi compartment, since the cleaved collagen and isolated N-terminal region can be detected in those locations and since the golgin Giantin is important for collagen processing [19,75–77]. However, uncleaved procollagen and N-proteinase activity also can be readily detected extracellularly in cell culture [4,20] and the best understood N-terminal proteinases, of the ADAMTS family, are secreted proteins also found extracellularly [78,79]. These latter observations led to the traditional view that N-terminal

processing occurs outside the cell. It is possible that processing normally occurs in both locations [3] and/or that partially processed and secreted collagens traffic through endocytic recycling compartments before final processing and matrix assembly [68].

Our data are more consistent with intracellular N-terminal cleavage of *C. elegans* cuticle collagens, since BLI-4 is mainly detected intracellularly and its loss leads to intracellular retention of SQT-3 and DPY-17. In most cases, the intracellular puncta appear to extend near to and potentially across the apical plasma membrane, suggesting that they could be present in tubulovesicular compartments that have access to the outside environment. Future identification of the BLI-4- and collagen-containing cellular compartments, combined with direct assays for cleavage and other modifications, should more precisely define the site and order of cuticle collagen processing. Ultimately, these studies should reveal how processing events help control the time and place of collagen assembly to construct the various cuticle structures and layers observed *in vivo*.

Methods

Strains and animal husbandry

See S1 Table for a list of all strains used in this work. *C. elegans* N2 was used as the wild-type strain. Unless otherwise indicated, strains were grown at 20˚C under standard conditions [80]. See S2 Table for specific mutant lesions and a list of all sgRNAs and primers used for genome editing or transgenics. Tagged collagen and BLI-4::SfGFP strains and CFCS mutants of *sqt-3* and *dpy-17* (RxxR to AxxA) were made by Suny Biotech (Fuzhou, China). The endogenous fusions are functional based on viability and normal body morphology of the homozygotes. Rescue transgene *csEx919 (bli-4+)* was generated by microinjection of fosmid WRM069bE05 (20 ng/ul) with *sur-5*::*GFP* (30 ng/ul) and bluescript SK+ (50 ng/ul).

Generation of *bli-4* alleles

Although *bli-4* null alleles had already been described [47,81], they were generated on chromosomes carrying other markers that could complicate analysis; therefore, we opted to generate new alleles in an N2 background. Mutant alleles were generated by CRISPR-Cas9 genome editing using methods described in [82] and the sgRNAs listed in S2 Table. N2 hermaphrodites were injected with sgRNAs (IDT), Cas9 (University of California Berkeley), and the marker pRF4, and F2 progeny were screened for expected embryonic or larval lethal phenotypes. Mutant alleles were recovered over a genetic balancer (either *hT2 (I;III)* or *szT1 (I;X)*) and then rescued with *bli-4*+ transgene *csEx919*. Mutant lesions were identified by PCR amplification and Sanger sequencing. We originally identified 4 putative *bli-4* null alleles, 8 putative *bli-4(c/d)* alleles, and 3 putative *bli-4(d)* alleles; however, only the alleles described here had small (<50 bp) deletions that permitted PCR-amplification with our methods, while the remaining alleles appeared to have larger deletions or rearrangements and were not further characterized.

Microscopy and image processing

For timelapse imaging, ~24 cell stage embryos were mounted in egg buffer/methyl cellulose with 20μM beads as spacers [83], incubated at 20˚ C for 4 hours, and then imaged using a stage temperature controller at 12˚ C and a Leica TCS SP5 confocal (20 z-planes at 0.5 μM spacing and 15 minute time spacing, total 16 hours). To immobilize animals for still imaging, embryos or larvae were suspended in M9 buffer with 10mM levamisole and mounted on 5% agarose pads supplemented with 20mM sodium azide. DIC and epifluorescence images were obtained with a Zeiss Axioskop (Carl Zeiss Microscopy) fitted with a Leica DFC360 FX camera with

Qcapture (Qimaging) software. Confocal images were captured with a Leica TCS SP8 confocal microscope, except for images in Figs 9C and 9D, and 10C and 10D, which were captured with a Zeiss LSM780 confocal microscope. Images were analyzed and processed in FIJI [84]. To quantify fusion protein accumulation in the extraembryonic space, fluorescence intensity was measured in a 3x3 μm region within a single medial confocal slice of each specimen. To quantify puncta number and size, maximum intensity projections were first thresholded with uniform settings and then the "analyze particles" function was used to identify particles between 0.05 and 3 microns^2 in area. For permeability assays, L1 larvae were incubated in 2 μg/ml Hoescht dye 33258 (Sigma) in M9 buffer for 15 minutes at room temperature, then washed twice with M9 before imaging.

Statistical analyses

Statistical analyses were performed using GraphPad Prism. In all dot-plots, lines and error bars indicate the median and range, respectively, and each dot represents a measurement from a single animal. To perform statistical analyses on quantitative measurement data, genotypes were compared using a non-parametric Mann-Whitney test. To perform statistical analyses on categorical data, phenotypes were classified as either normal or abnormal and then proportions compared using a two-tailed Fisher's Exact test. Raw data for all graphs can be found in Supporting data files 1–8.

bli-4 isoform analysis from single-cell RNA-seq data

scRNA-seq reads from [52] were remapped to each exon of the protein coding genes in Wormbase genome build WS277 using cellranger software (10x genomics). Only reads mapping to isoform-specific exons or 3' UTRs were considered in this analysis. The resulting UMI counts per exon for each tissue were combined in VisCello software with the existing *C. elegans* embryo scRNA-seq atlas [52]. Pseudobulk expression levels of each *bli-4* exon in reads per million were calculated in cells annotated as each cell type, and in major tissue classes as annotated in [52]. Code used for these analyses are available at Github: https://github.com/jisaacmurray/bli4_paper.

Western blots

Western blots with BLI-4::SfGFP(int) were performed as in [85] using primary antibody goat anti-GFP (Rockland Immunochemicals, 600-101-215, 1:1000 dilution) and secondary antibody anti-goat-HRP (Rockland Immunochemicals, 605–4302, 1:10,000 dilution). Embryos were collected from gravid adults via the alkaline bleach method and then allowed to develop for 5 hours in M9 before processing.

Supporting information

S1 Table. *C. elegans* strains used.
(XLSX)

S2 Table. Sequences of *bli-4* mutant alleles and insertions.
(XLSX)

S1 Fig. Pre-cuticle mCherry fusions accumulate in lysosome-like compartments following endocytosis. A,B) Pre-cuticle mCherry fusions, but not SfGFP fusions, mark large internal structures in late embryos (4 hours after 1.5-fold). A) *noah-1(mc68* [NOAH-1::mCherry(int)]*)* compared to *aaaIs25* [NOAH-1::SfGFP(int)]. B) *lpr-3(cs266* [ss::mCherry::LPR-3]) compared

to *lpr-3(cs250* [ss::SfGFP::LPR-3]*)*. All images are maximum intensity projections from confocal Z-slices and representative of at least 5 embryos per genotype. Scale bar, 10 microns.
(TIF)

S2 Fig. *bli-4* isoform expression in the embryo. Embryo scRNA-seq reads from [52] were mapped to the 3' ends of the various *bli-4* isoforms to estimate expression levels in the major tissue classes (Methods). RPM, reads per million. Our methods could not distinguish isoforms f and g, despite their different 3' coding regions, since these isoforms share a similar 3' UTR. The most highly expressed isoform in the embryo and in the epidermis was the CRD-containing isoform, *bli-4d*, with more modest levels of *bli-4a* and f/*g*, and negligible evidence for other isoforms. Note that comparing absolute levels of one isoform with another should be done with caution due to transcript specific biases, and the scRNA-seq data comprise exclusively cells from the first ~half of embryogenesis, so later differences in expression will not be captured.
(TIF)

S3 Fig. BLI-4 is dispensable for trafficking and apical membrane localization of the ZP protein NOAH-1. A) Schematic diagram of the NOAH-1::SfGFP(int) transgene fusion (*aaaIs25*) [87], which was used instead of the endogenous fusion because of chromosomal linkage of the *bli-4* and *noah-1* loci. The SfGFP tag (green triangle) is located between the Plasminogen (PAN) and ZP domains, as indicated. The C-terminal CFCS (RKKR, orange) is located before a predicted transmembrane (TM) domain. B) NOAH-1::SfGFP(int) appears similar between *WT* and *bli-4* mutant embryos (1.5-fold + 3 hour stage). Images are single confocal Z-slices and are representative of at least 10 embryos per genotype. C) Peak membrane fluorescence intensity was calculated with FIJI [84] using line scans across single confocal Z-slices, as shown in B. There was no significant difference (ns) among the genotypes.
(TIF)

S1 Video. Related to Fig 4D. Time-lapse video of an elongating *bli-4(cs281)* embryo, taken at 12˚C. Video is representative of at least 5 imaged specimens.
(MOV)

S2 Video. Related to Fig 4D. Time-lapse video of an elongating *bli-4(cs281); csEx919* rescued embryo, taken at 12˚C. Video is representative of at least 5 imaged specimens.
(MOV)

S1 Data. Source file for Fig 3E.
(XLSX)

S2 Data. Source file for Fig 4C.
(XLSX)

S3 Data. Source file for Fig 5A–5D.
(XLSX)

S4 Data. Source file for Fig 6C and 6D.
(XLSX)

S5 Data. Source file for Fig 7C and 7D.
(XLSX)

S6 Data. Source file for Fig 8C.
(XLSX)

S7 Data. Source file for Fig 9B and 9D.
(XLSX)

S8 Data. Source file for Fig 10D.
(XLSX)

S9 Data. Source file for S2 Fig.
(XLSX)

Acknowledgments

We thank Alison Frand and Michel Labouesse for strains, Andrea Stout and the Microscopy core at University of Pennsylvania for training and assistance with imaging, and Priya Sivaramakrishnan for assistance with time-lapse imaging. We thank colleagues at the 2023 Collagen Gordon Research Conference and Nathalie Pujol, Helen Schmidt, Nicholas Serra, and Trevor Barker for helpful discussions or comments on the manuscript, and Nathalie Pujol for hosting M.V.S. during the final stages of its preparation. Some strains used in this study were provided by the *Caenorhabditis* Genetics Center, which is funded by the NIH Office of Research Infrastructure Programs (P40 OD010440).

Author Contributions

Conceptualization: Jennifer D. Cohen, Andrew D. Chisholm, Meera V. Sundaram.

Data curation: Susanna K. Birnbaum, Meera V. Sundaram.

Formal analysis: Susanna K. Birnbaum, John I. Murray, Meera V. Sundaram.

Funding acquisition: Meera V. Sundaram.

Investigation: Susanna K. Birnbaum, Jennifer D. Cohen, Alexandra Belfi.

Methodology: Susanna K. Birnbaum.

Project administration: Meera V. Sundaram.

Resources: Jennifer R. G. Adams, Andrew D. Chisholm.

Supervision: Meera V. Sundaram.

Visualization: Susanna K. Birnbaum.

Writing – original draft: Meera V. Sundaram.

Writing – review & editing: Susanna K. Birnbaum, Jennifer D. Cohen, Alexandra Belfi, John I. Murray, Andrew D. Chisholm.

References

1. Furie B, Furie BC. The molecular basis of blood coagulation. Cell. 1988; 53: 505–518. https://doi.org/10.1016/0092-8674(88)90567-3 PMID: 3286010
2. Bokhove M, Jovine L. Structure of Zona Pellucida Module Proteins. Curr Top Dev Biol. 2018; 130: 413–442. https://doi.org/10.1016/bs.ctdb.2018.02.007 PMID: 29853186
3. Hellicar J, Stevenson NL, Stephens DJ, Lowe M. Supply chain logistics—the role of the Golgi complex in extracellular matrix production and maintenance. J Cell Sci. 2022; 135: jcs258879. https://doi.org/10.1242/jcs.258879 PMID: 35023559
4. Lichtenstein JR, Martin GR, Kohn LD, Byers PH, McKusick VA. Defect in conversion of procollagen to collagen in a form of Ehlers-Danlos syndrome. Science. 1973; 182: 298–300. https://doi.org/10.1126/science.182.4109.298 PMID: 4742738

5. Canty EG, Kadler KE. Procollagen trafficking, processing and fibrillogenesis. J Cell Sci. 2005; 118: 1341–1353. https://doi.org/10.1242/jcs.01731 PMID: 15788652

6. Kadler KE. Fell Muir Lecture: Collagen fibril formation in vitro and in vivo. Int J Exp Pathol. 2017; 98: 4–16. https://doi.org/10.1111/iep.12224 PMID: 28508516

7. Revell CK, Jensen OE, Shearer T, Lu Y, Holmes DF, Kadler KE. Collagen fibril assembly: New approaches to unanswered questions. Matrix Biol Plus. 2021; 12: 100079. https://doi.org/10.1016/j.mbplus.2021.100079 PMID: 34381990

8. Kessler E, Takahara K, Biniaminov L, Brusel M, Greenspan DS. Bone morphogenetic protein-1: the type I procollagen C-proteinase. Science. 1996; 271: 360–362. https://doi.org/10.1126/science.271.5247.360 PMID: 8553073

9. Colige A, Sieron AL, Li SW, Schwarze U, Petty E, Wertelecki W, et al. Human Ehlers-Danlos syndrome type VII C and bovine dermatosparaxis are caused by mutations in the procollagen I N-proteinase gene. Am J Hum Genet. 1999; 65: 308–317. https://doi.org/10.1086/302504 PMID: 10417273

10. Lindahl K, Barnes AM, Fratzl-Zelman N, Whyte MP, Hefferan TE, Makareeva E, et al. COL1 C-propeptide cleavage site mutations cause high bone mass osteogenesis imperfecta. Hum Mutat. 2011; 32: 598–609. https://doi.org/10.1002/humu.21475 PMID: 21344539

11. Byers PH, Duvic M, Atkinson M, Robinow M, Smith LT, Krane SM, et al. Ehlers-Danlos syndrome type VIIA and VIIB result from splice-junction mutations or genomic deletions that involve exon 6 in the COL1A1 and COL1A2 genes of type I collagen. Am J Med Genet. 1997; 72: 94–105. https://doi.org/10.1002/(sici)1096-8628(19971003)72:1<94::aid-ajmg20>3.0.co;2-o PMID: 9295084

12. Malfait F, Symoens S, Goemans N, Gyftodimou Y, Holmberg E, López-González V, et al. Helical mutations in type I collagen that affect the processing of the amino-propeptide result in an Osteogenesis Imperfecta/Ehlers-Danlos Syndrome overlap syndrome. Orphanet J Rare Dis. 2013; 8: 78. https://doi.org/10.1186/1750-1172-8-78 PMID: 23692737

13. Yang J, Kramer JM. In vitro mutagenesis of Caenorhabditis elegans cuticle collagens identifies a potential subtilisin-like protease cleavage site and demonstrates that carboxyl domain disulfide bonding is required for normal function but not assembly. Mol Cell Biol. 1994; 14: 2722–2730. https://doi.org/10.1128/mcb.14.4.2722-2730.1994 PMID: 8139571

14. Yang J, Kramer JM. Proteolytic processing of Caenorhabditis elegans SQT-1 cuticle collagen is inhibited in right roller mutants whereas cross-linking is inhibited in left roller mutants. J Biol Chem. 1999; 274: 32744–32749. https://doi.org/10.1074/jbc.274.46.32744 PMID: 10551833

15. Snellman A, Tu H, Väisänen T, Kvist AP, Huhtala P, Pihlajaniemi T. A short sequence in the N-terminal region is required for the trimerization of type XIII collagen and is conserved in other collagenous transmembrane proteins. EMBO J. 2000; 19: 5051–5059. https://doi.org/10.1093/emboj/19.19.5051 PMID: 11013208

16. Wakabayashi T. Transmembrane Collagens in Neuromuscular Development and Disorders. Front Mol Neurosci. 2020; 13: 635375. https://doi.org/10.3389/fnmol.2020.635375 PMID: 33536873

17. Tu H, Huhtala P, Lee H-M, Adams JC, Pihlajaniemi T. Membrane-associated collagens with interrupted triple-helices (MACITs): evolution from a bilaterian common ancestor and functional conservation in C. elegans. BMC Evol Biol. 2015; 15: 281. https://doi.org/10.1186/s12862-015-0554-3 PMID: 26667623

18. Kadler KE, Hojima Y, Prockop DJ. Assembly of collagen fibrils de novo by cleavage of the type I pC-collagen with procollagen C-proteinase. Assay of critical concentration demonstrates that collagen self-assembly is a classical example of an entropy-driven process. J Biol Chem. 1987; 262: 15696–15701. PMID: 3316206

19. Tanaka T, Moriya K, Tsunenaga M, Yanagawa T, Morita H, Minowa T, et al. Visualized procollagen Iα1 demonstrates the intracellular processing of propeptides. Life Sci Alliance. 2022; 5: e202101060. https://doi.org/10.26508/lsa.202101060 PMID: 35181633

20. Bruns RR, Hulmes DJ, Therrien SF, Gross J. Procollagen segment-long-spacing crystallites: their role in collagen fibrillogenesis. Proc Natl Acad Sci U S A. 1979; 76: 313–317. https://doi.org/10.1073/pnas.76.1.313 PMID: 284347

21. Hulmes DJ, Kadler KE, Mould AP, Hojima Y, Holmes DF, Cummings C, et al. Pleomorphism in type I collagen fibrils produced by persistence of the procollagen N-propeptide. J Mol Biol. 1989; 210: 337–345. https://doi.org/10.1016/0022-2836(89)90335-5 PMID: 2600969

22. Holmes DF, Watson RB, Steinmann B, Kadler KE. Ehlers-Danlos syndrome type VIIB. Morphology of type I collagen fibrils formed in vivo and in vitro is determined by the conformation of the retained N-propeptide. J Biol Chem. 1993; 268: 15758–15765. PMID: 8340401

23. Ricard-Blum S. The collagen family. Cold Spring Harb Perspect Biol. 2011; 3: a004978. https://doi.org/10.1101/cshperspect.a004978 PMID: 21421911

24. Harrington MJ, Waite JH. pH-dependent locking of giant mesogens in fibers drawn from mussel byssal collagens. Biomacromolecules. 2008; 9: 1480–1486. https://doi.org/10.1021/bm8000827 PMID: 18402475

25. Thacker C, Sheps JA, Rose AM. Caenorhabditis elegans dpy-5 is a cuticle procollagen processed by a proprotein convertase. Cell Mol Life Sci. 2006; 63: 1193–1204. https://doi.org/10.1007/s00018-006-6012-z PMID: 16649143

26. Page AP, Johnstone IL. The cuticle. WormBook. 2007; 1–15. https://doi.org/10.1895/wormbook.1.138.1 PMID: 18050497

27. Teuscher AC, Jongsma E, Davis MN, Statzer C, Gebauer JM, Naba A, et al. The in-silico characterization of the Caenorhabditis elegans matrisome and proposal of a novel collagen classification. Matrix Biol Plus. 2019; 1: 100001. https://doi.org/10.1016/j.mbplus.2018.11.001 PMID: 33543001

28. Mancuso VP, Parry JM, Storer L, Poggioli C, Nguyen KCQ, Hall DH, et al. Extracellular leucine-rich repeat proteins are required to organize the apical extracellular matrix and maintain epithelial junction integrity in C. elegans. Development. 2012; 139: 979–990. https://doi.org/10.1242/dev.075135 PMID: 22278925

29. Kelley M, Yochem J, Krieg M, Calixto A, Heiman MG, Kuzmanov A, et al. FBN-1, a fibrillin-related protein, is required for resistance of the epidermis to mechanical deformation during C. elegans embryogenesis. Elife. 2015;4. https://doi.org/10.7554/eLife.06565 PMID: 25798732

30. Gill HK, Cohen JD, Ayala-Figueroa J, Forman-Rubinsky R, Poggioli C, Bickard K, et al. Integrity of Narrow Epithelial Tubes in the C. elegans Excretory System Requires a Transient Luminal Matrix. PLoS Genet. 2016; 12: e1006205. https://doi.org/10.1371/journal.pgen.1006205 PMID: 27482894

31. Forman-Rubinsky R, Cohen JD, Sundaram MV. Lipocalins Are Required for Apical Extracellular Matrix Organization and Remodeling in Caenorhabditis elegans. Genetics. 2017; 207: 625–642. https://doi.org/10.1534/genetics.117.300207 PMID: 28842397

32. Vuong-Brender TTK, Suman SK, Labouesse M. The apical ECM preserves embryonic integrity and distributes mechanical stress during morphogenesis. Development. 2017; 144: 4336–4349. https://doi.org/10.1242/dev.150383 PMID: 28526752

33. Cohen JD, Flatt KM, Schroeder NE, Sundaram MV. Epithelial Shaping by Diverse Apical Extracellular Matrices Requires the Nidogen Domain Protein DEX-1 in Caenorhabditis elegans. Genetics. 2019; 211: 185–200. https://doi.org/10.1534/genetics.118.301752 PMID: 30409789

34. Cohen JD, Sparacio AP, Belfi AC, Forman-Rubinsky R, Hall DH, Maul-Newby H, et al. A multi-layered and dynamic apical extracellular matrix shapes the vulva lumen in Caenorhabditis elegans. Elife. 2020; 9: e57874. https://doi.org/10.7554/eLife.57874 PMID: 32975517

35. Johnstone IL, Barry JD. Temporal reiteration of a precise gene expression pattern during nematode development. EMBO J. 1996; 15: 3633–3639. PMID: 8670866

36. Hendriks G-J, Gaidatzis D, Aeschimann F, Großhans H. Extensive oscillatory gene expression during C. elegans larval development. Mol Cell. 2014; 53: 380–392. https://doi.org/10.1016/j.molcel.2013.12.013 PMID: 24440504

37. Meeuse MW, Hauser YP, Morales Moya LJ, Hendriks G-J, Eglinger J, Bogaarts G, et al. Developmental function and state transitions of a gene expression oscillator in Caenorhabditis elegans. Mol Syst Biol. 2020; 16: e9498. https://doi.org/10.15252/msb.20209498 PMID: 32687264

38. Frand AR, Russel S, Ruvkun G. Functional genomic analysis of C. elegans molting. PLoS Biol. 2005; 3: e312. https://doi.org/10.1371/journal.pbio.0030312 PMID: 16122351

39. Lažetić V, Fay DS. Molting in C. elegans. Worm. 2017; 6: e1330246. https://doi.org/10.1080/21624054.2017.1330246 PMID: 28702275

40. Joseph BB, Wang Y, Edeen P, Lažetić V, Grant BD, Fay DS. Control of clathrin-mediated endocytosis by NIMA family kinases. PLoS Genet. 2020; 16: e1008633. https://doi.org/10.1371/journal.pgen.1008633 PMID: 32069276

41. Joseph BB, Edeen PT, Meadows S, Binti S, Fay DS. An unexpected role for the conserved ADAM-family metalloprotease ADM-2 in Caenorhabditis elegans molting. PLoS Genet. 2022; 18: e1010249. https://doi.org/10.1371/journal.pgen.1010249 PMID: 35639786

42. Zhang Z, Bai M, Barbosa GO, Chen A, Wei Y, Luo S, et al. Broadly conserved roles of TMEM131 family proteins in intracellular collagen assembly and secretory cargo trafficking. Sci Adv. 2020; 6: eaay7667. https://doi.org/10.1126/sciadv.aay7667 PMID: 32095531

43. Zhang Z, Luo S, Barbosa GO, Bai M, Kornberg TB, Ma DK. The conserved transmembrane protein TMEM-39 coordinates with COPII to promote collagen secretion and regulate ER stress response. PLoS Genet. 2021; 17: e1009317. https://doi.org/10.1371/journal.pgen.1009317 PMID: 33524011

44. Novelli J, Ahmed S, Hodgkin J. Gene interactions in Caenorhabditis elegans define DPY-31 as a candidate procollagen C-proteinase and SQT-3/ROL-4 as its predicted major target. Genetics. 2004; 168: 1259–1273. https://doi.org/10.1534/genetics.104.027953 PMID: 15579684

45. Novelli J, Page AP, Hodgkin J. The C terminus of collagen SQT-3 has complex and essential functions in nematode collagen assembly. Genetics. 2006; 172: 2253–2267. https://doi.org/10.1534/genetics.105.053637 PMID: 16452136

46. Stepek G, McCormack G, Page AP. Collagen processing and cuticle formation is catalysed by the astacin metalloprotease DPY-31 in free-living and parasitic nematodes. Int J Parasitol. 2010; 40: 533–542. https://doi.org/10.1016/j.ijpara.2009.10.007 PMID: 19883650

47. Thacker C, Peters K, Srayko M, Rose AM. The bli-4 locus of Caenorhabditis elegans encodes structurally distinct kex2/subtilisin-like endoproteases essential for early development and adult morphology. Genes Dev. 1995; 9: 956–71. https://doi.org/10.1101/gad.9.8.956 PMID: 7774813

48. Seidah NG, Prat A. The biology and therapeutic targeting of the proprotein convertases. Nat Rev Drug Discov. 2012; 11: 367–383. https://doi.org/10.1038/nrd3699 PMID: 22679642

49. Nour N, Mayer G, Mort JS, Salvas A, Mbikay M, Morrison CJ, et al. The cysteine-rich domain of the secreted proprotein convertases PC5A and PACE4 functions as a cell surface anchor and interacts with tissue inhibitors of metalloproteinases. Mol Biol Cell. 2005; 16: 5215–5226. https://doi.org/10.1091/mbc.e05-06-0504 PMID: 16135528

50. Mayer G, Hamelin J, Asselin M-C, Pasquato A, Marcinkiewicz E, Tang M, et al. The regulated cell surface zymogen activation of the proprotein convertase PC5A directs the processing of its secretory substrates. J Biol Chem. 2008; 283: 2373–2384. https://doi.org/10.1074/jbc.M708763200 PMID: 18039650

51. Cao J, Packer JS, Ramani V, Cusanovich DA, Huynh C, Daza R, et al. Comprehensive single-cell transcriptional profiling of a multicellular organism. Science. 2017; 357: 661–667. https://doi.org/10.1126/science.aam8940 PMID: 28818938

52. Packer JS, Zhu Q, Huynh C, Sivaramakrishnan P, Preston E, Dueck H, et al. A lineage-resolved molecular atlas of C. elegans embryogenesis at single-cell resolution. Science. 2019; 365: eaax1971. https://doi.org/10.1126/science.aax1971 PMID: 31488706

53. Taylor SR, Santpere G, Weinreb A, Barrett A, Reilly MB, Xu C, et al. Molecular topography of an entire nervous system. Cell. 2021; 184: 4329–4347.e23. https://doi.org/10.1016/j.cell.2021.06.023 PMID: 34237253

54. Kass J, Jacob TC, Kim P, Kaplan JM. The EGL-3 proprotein convertase regulates mechanosensory responses of Caenorhabditis elegans. J Neurosci. 2001; 21: 9265–9272. https://doi.org/10.1523/JNEUROSCI.21-23-09265.2001 PMID: 11717360

55. Mahoney TR, Luo S, Round EK, Brauner M, Gottschalk A, Thomas JH, et al. Intestinal signaling to GABAergic neurons regulates a rhythmic behavior in Caenorhabditis elegans. Proc Natl Acad Sci U S A. 2008; 105: 16350–16355. https://doi.org/10.1073/pnas.0803617105 PMID: 18852466

56. Schroeder NE, Androwski RJ, Rashid A, Lee H, Lee J, Barr MM. Dauer-specific dendrite arborization in C. elegans is regulated by KPC-1/Furin. Curr Biol. 2013; 23: 1527–1535. https://doi.org/10.1016/j.cub.2013.06.058 PMID: 23932402

57. Cohen JD, Sundaram MV. C. elegans Apical Extracellular Matrices Shape Epithelia. J Dev Biol. 2020; 8: E23. https://doi.org/10.3390/jdb8040023 PMID: 33036165

58. Priess JR, Hirsh DI. Caenorhabditis elegans morphogenesis: the role of the cytoskeleton in elongation of the embryo. Dev Biol. 1986; 117: 156–173. https://doi.org/10.1016/0012-1606(86)90358-1 PMID: 3743895

59. Clancy JC, Vo AA, Myles KM, Levenson MT, Ragle JM, Ward JD. Experimental considerations for study of C. elegans lysosomal proteins. G3 (Bethesda). 2023; 13: jkad032. https://doi.org/10.1093/g3journal/jkad032 PMID: 36748711

60. Sulston JE, Schierenberg E, White JG, Thomson JN. The embryonic cell lineage of the nematode Caenorhabditis elegans. Dev Biol. 1983; 100: 64–119. https://doi.org/10.1016/0012-1606(83)90201-4 PMID: 6684600

61. McKay SJ, Johnsen R, Khattra J, Asano J, Baillie DL, Chan S, et al. Gene expression profiling of cells, tissues, and developmental stages of the nematode C. elegans. Cold Spring Harb Symp Quant Biol. 2003; 68: 159–169. https://doi.org/10.1101/sqb.2003.68.159 PMID: 15338614

62. Kusch M, Edgar RS. Genetic studies of unusual loci that affect body shape of the nematode Caenorhabditis elegans and may code for cuticle structural proteins. Genetics. 1986; 113: 621–639. https://doi.org/10.1093/genetics/113.3.621 PMID: 3732788

63. Thein MC, McCormack G, Winter AD, Johnstone IL, Shoemaker CB, Page AP. Caenorhabditis elegans exoskeleton collagen COL-19: an adult-specific marker for collagen modification and assembly, and the

analysis of organismal morphology. Dev Dyn. 2003; 226: 523–539. https://doi.org/10.1002/dvdy.10259 PMID: 12619137

64. Lang AE, Lundquist EA. The Collagens DPY-17 and SQT-3 Direct Anterior-Posterior Migration of the Q Neuroblasts in C. elegans. J Dev Biol. 2021; 9: 7. https://doi.org/10.3390/jdb9010007 PMID: 33669899

65. Buchler NE, Gerland U, Hwa T. Nonlinear protein degradation and the function of genetic circuits. Proc Natl Acad Sci U S A. 2005; 102: 9559–9564. https://doi.org/10.1073/pnas.0409553102 PMID: 15972813

66. Costa M, Draper BW, Priess JR. The role of actin filaments in patterning the Caenorhabditis elegans cuticle. Dev Biol. 1997; 184: 373–384. https://doi.org/10.1006/dbio.1997.8530 PMID: 9133443

67. Johnstone IL. Cuticle collagen genes. Expression in Caenorhabditis elegans. Trends Genet. 2000; 16: 21–27. https://doi.org/10.1016/s0168-9525(99)01857-0 PMID: 10637627

68. Chang J, Pickard A, Garva R, Lu Y, Gullberg D, Kadler KE. The endosome is a master regulator of plasma membrane collagen fibril assembly. biorxiv. 2021;https://doi.org/10.1101/2021.03.25.436925.

69. McMahon L, Muriel JM, Roberts B, Quinn M, Johnstone IL. Two sets of interacting collagens form functionally distinct substructures within a Caenorhabditis elegans extracellular matrix. Mol Biol Cell. 2003; 14: 1366–1378. https://doi.org/10.1091/mbc.e02-08-0479 PMID: 12686594

70. Areida SK, Reinhardt DP, Muller PK, Fietzek PP, Kowitz J, Marinkovich MP, et al. Properties of the collagen type XVII ectodomain. Evidence for n- to c-terminal triple helix folding. J Biol Chem. 2001; 276: 1594–1601. https://doi.org/10.1074/jbc.M008709200 PMID: 11042218

71. McAlinden A, Smith TA, Sandell LJ, Ficheux D, Parry DAD, Hulmes DJS. Alpha-helical coiled-coil oligomerization domains are almost ubiquitous in the collagen superfamily. J Biol Chem. 2003; 278: 42200–42207. https://doi.org/10.1074/jbc.M302429200 PMID: 12920133

72. Edens WA, Sharling L, Cheng G, Shapira R, Kinkade JM, Lee T, et al. Tyrosine cross-linking of extracellular matrix is catalyzed by Duox, a multidomain oxidase/peroxidase with homology to the phagocyte oxidase subunit gp91phox. J Cell Biol. 2001; 154: 879–891. https://doi.org/10.1083/jcb.200103132 PMID: 11514595

73. Thein MC, Winter AD, Stepek G, McCormack G, Stapleton G, Johnstone IL, et al. Combined extracellular matrix cross-linking activity of the peroxidase MLT-7 and the dual oxidase BLI-3 is critical for post-embryonic viability in Caenorhabditis elegans. J Biol Chem. 2009; 284: 17549–17563. https://doi.org/10.1074/jbc.M900831200 PMID: 19406744

74. Miao R, Li M, Zhang Q, Yang C, Wang X. An ECM-to-Nucleus Signaling Pathway Activates Lysosomes for C. elegans Larval Development. Dev Cell. 2020; 52: 21–37.e5. https://doi.org/10.1016/j.devcel.2019.10.020 PMID: 31735670

75. Humphries SM, Lu Y, Canty EG, Kadler KE. Active negative control of collagen fibrillogenesis in vivo. Intracellular cleavage of the type I procollagen propeptides in tendon fibroblasts without intracellular fibrils. J Biol Chem. 2008; 283: 12129–12135. https://doi.org/10.1074/jbc.M708198200 PMID: 18285337

76. Canty-Laird EG, Lu Y, Kadler KE. Stepwise proteolytic activation of type I procollagen to collagen within the secretory pathway of tendon fibroblasts in situ. Biochem J. 2012; 441: 707–717. https://doi.org/10.1042/BJ20111379 PMID: 21967573

77. Stevenson NL, Bergen DJM, Lu Y, Prada-Sanchez ME, Kadler KE, Hammond CL, et al. Giantin is required for intracellular N-terminal processing of type I procollagen. J Cell Biol. 2021; 220: e202005166. https://doi.org/10.1083/jcb.202005166 PMID: 33944912

78. Dubail J, Apte SS. Insights on ADAMTS proteases and ADAMTS-like proteins from mammalian genetics. Matrix Biol. 2015;44–46: 24–37. https://doi.org/10.1016/j.matbio.2015.03.001 PMID: 25770910

79. Bekhouche M, Colige A. The procollagen N-proteinases ADAMTS2, 3 and 14 in pathophysiology. Matrix Biol. 2015;44–46: 46–53. https://doi.org/10.1016/j.matbio.2015.04.001 PMID: 25863161

80. Brenner S. The genetics of Caenorhabditis elegans. Genetics. 1974; 77: 71–94. https://doi.org/10.1093/genetics/77.1.71 PMID: 4366476

81. Thacker C, Srayko M, Rose AM. Mutational analysis of bli-4/kpc-4 reveals critical residues required for proprotein convertase function in C. elegans. Gene. 2000; 252: 15–25. https://doi.org/10.1016/s0378-1119(00)00211-0 PMID: 10903434

82. Dokshin GA, Ghanta KS, Piscopo KM, Mello CC. Robust Genome Editing with Short Single-Stranded and Long, Partially Single-Stranded DNA Donors in Caenorhabditis elegans. Genetics. 2018; 210: 781–787. https://doi.org/10.1534/genetics.118.301532 PMID: 30213854

83. Bao Z, Murray JI. Mounting Caenorhabditis elegans embryos for live imaging of embryogenesis. Cold Spring Harb Protoc. 2011; 2011: pdb.prot065599. https://doi.org/10.1101/pdb.prot065599 PMID: 21880814

84. Schindelin J, Arganda-Carreras I, Frise E, Kaynig V, Longair M, Pietzsch T, et al. Fiji: an open-source platform for biological-image analysis. Nature Methods. 2012; 9: 676–82. https://doi.org/10.1038/nmeth.2019 PMID: 22743772

85. Cohen JD, Bermudez JG, Good MC, Sundaram MV. A C. elegans Zona Pellucida domain protein functions via its ZPc domain. PLoS Genet. 2020; 16: e1009188. https://doi.org/10.1371/journal.pgen.1009188 PMID: 33141826

86. Winter AD, Page AP. Prolyl 4-Hydroxylase Is an Essential Procollagen-Modifying Enzyme Required for Exoskeleton Formation and the Maintenance of Body Shape in the Nematode Caenorhabditis elegans. Mol Cell Biol. 2000; 20: 4084–4093. https://doi.org/10.1128/MCB.20.11.4084-4093.2000 PMID: 10805750

87. Katz SS, Barker TJ, Maul-Newby HM, Sparacio AP, Nguyen KCQ, Maybrun CL, et al. A transient apical extracellular matrix relays cytoskeletal patterns to shape permanent acellular ridges on the surface of adult C. elegans. PLoS Genet. 2022; 18: e1010348. https://doi.org/10.1371/journal.pgen.1010348 PMID: 35960773